Strål
säkerhets
myndigheten
Swedish Radiation Safety Authority

Authors: Richard Becker[1]
Antti Forsström[2]
Yuriy Yagodzinskyy[2]
Hannu Hänninen[2]
Mikko Heikkilä[3]

1. Studsvik Nuclear AB, Sweden
2. Aalto University, School of Engineering,
Department of Mechanical Engineering, Espoo, Finland
3. Helsinki University, Faculty of Science,
Department of Chemistry, Helsinki, Finland

Research

2020:01

Sulphide-induced stress corrosion cracking and hydrogen absorption in copper exposed to sulphide and chloride containing deoxygenated water at 90°C

Report number: 2020:01 **ISSN:** 2000-0456
Available at www.stralsakerhetsmyndigheten.se

SSM perspektiv

Bakgrund

Den metod som den svenska kärnkraftsindustrin planerar att tillämpa för att slutförvara använt kärnbränsle kallas för KBS-3 och bygger på tre skyddsbarriärer: kopparkapslar, bentonitbuffert och det svenska urberget. I den aktuella KBS-3-utformningen kommer det använda kärnbränslet att placeras i en insats av gjutjärn som omgärdas av ett 50 mm tjockt kopparhölje. Gjutjärnsinsatsen ger mekanisk hållfasthet och strålskydd, medan kopparhöljet utgör kapselns korrosionsbarriär. Kapseln ska sedan deponeras i ett förvar i Forsmarks urberg på ett djup på ca 500 m, där varje kapsel omsluts av en bentonitbuffert, främst för att begränsa transport av grundvatten till och från kapselytan. Vid utvärdering av KBS-3-systemets långsiktiga skyddsförmåga är förståelsen för långtidsutvecklingen av processer som kan påverka kapselns inneslutningsfunktion, till exempel lokala korrosionsprocesser såsom spänningskorrosion och gropkorrosion under reducerande kemiska betingelser, av stor vikt. Forskningsstudier som kan bidra till att belysa förutsättningar och utöka förståelsen för dessa typer av fundamentala processer och mekanismer utgör därför viktiga underlag i sammanhanget. För att avgöra betydelsen av enskilda resultat för bedömningen av ett KBS-3-slutförvars långsiktiga strålsäkerhet kräver dock ett beaktande av aktuell slutförvarsmiljös förhållanden och långsiktiga utveckling och de i detta sammanhang för processen viktigaste parametrarna. För gropkorrosion under reducerande betingelser är dessa i första hand koncentrationer och flux av vätesulfidjoner, samt även kloridhalt, vilka kräver en förståelse och analys av både grundvattenkemiska förhållanden och transportprocesser i kapselns närhet. För spänningskorrosion, vilket även förutsätter förekomst av dragspänningar i höljet, fordras också, utöver parametrarna som styr förutsättningarna för gropkorrosion i slutförvarsmiljö, en förståelse av lasterna som kan förekomma i slutförvaret samt utvecklingen av spänningsförhållanden i kapseln.

Resultat

Spänningskorrosion av OFP-koppar i reducerande sulfidmiljö har studerats med SSRT-metoden, i vilken kopparproverna utsätts för dragspänningar under långsam belastning, vid 90 oC och olika sulfidkoncentrationer (0,001 M respektive 0,00001 M). Vid den högre sulfidkoncentrationen observerades interkristallina defekter i kopparmaterialet vilket inte noterades i prover som exponerats vid den lägre sulfidkoncentrationen. I samma försöksmiljö exponerades även obelastade kopparprover, både basmaterial och koppar från svetsat material, för att utröna effekten av mekanisk pålastning på omfattningen av väteladdning i kopparmaterialet. Högst väteladdning observerades i de obelastade, svetsade kopparproverna. För basmaterialet konstaterades att mekaniskt laddade kopparprover uppvisar en något högre vätehalt efter exponering än de obelastade proverna. För obelastade prover exponerade vid den lägre sulfidkoncentrationen noterades en lägre vätehalt efter exponering än före. Det observerades att sulfideringen av oxidfilmer som bildats på

kopparproverna före exponering var väldigt effektiv. En utförligare sammanfattning av resultaten återfinns i ”Summary” i inledningen av rapporten.

Relevans

Detta forskningsprojekt är en fortsättning på en SSM-finansierad studie (SSM 2017:02) som syftade till att belysa kemiska och mekaniska förutsättningar för spänningskorrosion av syrefri, fosfordopad koppar, så kallad OFP-koppar, i sulfidmiljö under kemiskt reducerande förhållanden genom långsam belastning av kopparprover i lösningar med varierad sulfidkoncentration (SSRT; Slow strain rate testing). Denna fortsättningsstudie fokuserar på att bekräfta och noggrannare inringa de gränsvärden på sulfidkoncentration och dragspänningar under vilka spänningskorrosion inte kunde observeras i det föregående projektet, samt även studera omfattningen av väteladdning som följd av sulfidkorrosion i både pålastade och obelastade kopparprover.

Behov av vidare forskning

Spänningskorrosion är en lokal korrosionsform som är förhållandevis komplex då den innefattar en samverkan mellan kemiska och mekaniska förhållanden. Föreliggande studie har bidragit till att uppskatta både kemiska, främst sulfidkoncentration, och mekaniska gränsvärden under vilka processen inte kan observeras. Mot bakgrund av spänningskorrosionsprocessers komplexitet anser SSM att det finns en relevans av att fortsatt studera spänningskorrosion av koppar under kemiskt reducerande betingelser, liksom processens mekanistiska förutsättningar samt även mekanismer för väteladdning av koppar. En ur ett KBS-3-slutförvarsperspektiv relevant inriktning skulle kunna innefatta experimentella studier med högre känslighet och detektionsförmåga som simulerar väteladdning av koppar i slutförvarsmiljö, samt inverkan av väteladdning i perspektivet spänningskorrosion.

Projektinformation

Kontaktperson SSM: Henrik Öberg
Referens: SSM2018-2132 / 3030045-44

SSM perspective

Background

The concept that the Swedish nuclear power industry plans to utilise for the final disposal spent nuclear fuel is called KBS-3 method, which is based on three different barriers to prevent spreading of radioactive substances: copper canisters, bentonite buffers and the surrounding Swedish bedrock. In the current KBS-3 design, the spent nuclear fuel will be placed in cast iron inserts which will be protected by a 50 mm thick copper shell. The cast iron insert provides mechanical strength and radiation shielding, while the copper constitutes the corrosion barrier of the canister. The canisters should then deposited in a repository at the Forsmark site at a depth of about 500 m, where each canister is enclosed by a bentonite buffer, primarily to limit transport of groundwater to and from the canister's surface. When evaluating The KBS-3 system's long-term protective capability, the understanding of long-term processes that can affect the canister containment function, for example, local corrosion processes such as stress corrosion cracking and pitting corrosion under reducing chemical conditions, is of great importance. Research studies can help elucidate conditions and expand understanding of these types of fundamental processes and mechanisms, which therefore constitute important evidence in this context. To determine the meaning of individual experimental results for the assessment of a long-term KBS-3 repository performance however, the radiation safety analysis requires consideration of the current environmental conditions in the repository environment, and the long-term development of those conditions, which in this context are represented by the most important parameters for the processes. For pitting corrosion during reducing conditions, those are primarily concentrations and fluxes of hydrogensulphide ions, as well as the chloride content, which need to be based on understanding and analysis of both groundwater chemical conditions and transport processes in the vicinity of a canister. For stress corrosion cracking, which additionally requires occurrence of tensile stresses in the shell in addition to the parameters controlling the conditions for pitting corrosion in the repository environment, such parameters need to be based on an understanding of the loading conditions that may occur in the repository as well as the development of stresses in the canister shell.

Results

Stress corrosion of OFP copper in a reducing sulphide environment has been studied with the SSRT method, in which the copper samples are subjected to tensile stresses under slow loading conditions, at 90°C and at the same time exposed for different sulphide concentrations (0.001 M and 0.00001 M, respectively). At the higher sulphide concentration level, intercrystalline defects in the copper material were observed, which was not the case for the samples exposed at the lower sulphide concentration level. Unloaded samples from copper base material as well as from welded copper material were also exposed in the same experi-

mental environment, in order to determine the effect of mechanical loading on the extent of hydrogen charging of the copper material. The highest hydrogen charging was observed in the unloaded welded copper samples. For the base material it was found that mechanically loaded copper samples exhibit a slightly higher hydrogen content after exposure as compared with the unloaded samples. For the unloaded samples exposed at the lower the sulphide concentration level, it was noted that hydrogen content was lower after exposure compared to before exposure. It was observed that the sulphidation of oxide films formed on the copper samples before exposure were very effective. A more detailed summary of the results can be found in "Summary" section in the beginning of the report.

Relevance

This research project is a continuation of an SSM-funded study (SSM 2017: 02) aimed at elucidating chemical and mechanical conditions required for stress corrosion of oxygen-free, phosphorus-doped copper, so-called OFP copper, in a sulphide environment under chemically reducing conditions by slow loading of copper samples in solutions with varied sulphide concentration (SSRT; Slow Strain Rate Testing). This continuation study focuses on confirming and more accurately establishing the limiting values for sulphide concentration and tensile stress, below which stress corrosion could not be observed in the previous project, and also to study the extent of hydrogen charging as a result of sulphide corrosion in both loaded and unloaded copper samples.

Need for further research

Stress corrosion is a form of local corrosion that can be regarded as complex as it involves an interaction between both chemical and mechanical conditions. The present study has contributed to estimating both chemical, mainly sulphide concentration, and mechanical limiting values below which the process cannot be observed. Considering the complexity of stress corrosion as a process, SSM considers it to be relevant to continue these studies under chemical reducing conditions, along with the mechanical conditions related to the process, as well as also covering mechanisms for the hydrogen loading of copper. A direction of these studies, based on a KBS-3 final repository relevance, could be experimental studies aimed at higher sensitivity and detection capability which simulate hydrogen charging of copper corresponding to the final repository environment, as well as the effect of hydrogen charging in the perspective of stress corrosion.

Projektinformation

Kontaktperson SSM: Henrik Öberg
Referens: SSM2018-2132 / 3030045-44

Strål
säkerhets
myndigheten
Swedish Radiation Safety Authority

Authors: Richard Becker[1]
Antti Forsström[2]
Yuriy Yagodzinskyy[2]
Hannu Hänninen[2]
Mikko Heikkilä[3]

1. Studsvik Nuclear AB, Sweden
2. Aalto University, School of Engineering,
Department of Mechanical Engineering, Espoo, Finland
3. Helsinki University, Faculty of Science,
Department of Chemistry, Helsinki, Finland

2020:01

Sulphide-induced stress corrosion cracking and hydrogen absorption in copper exposed to sulphide and chloride containing deoxygenated water at 90°C

Date: February 2020
Report number: 2020:01 **ISSN:** 2000-0456
Available at www.stralsakerhetsmyndigheten.se

This report concerns a study which has been conducted for the Swedish Radiation Safety Authority, SSM. The conclusions and viewpoints presented in the report are those of the author/authors and do not necessarily coincide with those of the SSM.

SSM 2020:01

Sulphide-induced stress corrosion cracking and hydrogen absorption in copper exposed to sulphide and chloride containing deoxygenated water at 90°C

Richard Becker[1], Antti Forsström[2], Yuriy Yagodzinskyy[2], Mikko Heikkilä[3], Hannu Hänninen[2]

1. Studsvik Nuclear AB, Sweden
2. Aalto University, School of Engineering, Department of Mechanical Engineering, Espoo, Finland
3. Helsinki University, Faculty of Science, Department of Chemistry, Helsinki, Finland

Table of Contents

1. Introduction and background 3
2. Experimental work 4
2.1. Test materials and specimens 4
2.2. Autoclave exposures 5
2.3. Specimen examination 6
2.4. Hydrogen thermal desorption spectroscopy (TDS) 7
2.5. X-ray diffraction (XRD) 7
3. Results 8
3.1. SSRT specimen exposed to the high sulphide environment (exposure #8) 8
3.1.1. Optical and SEM observations 8
3.1.2. EBSD of the surface defects 15
3.2. SSRT specimen exposed to the low sulphide environment (exposure #9) 17
3.2.1. Optical and SEM observations 17
3.3. Unloaded coupon specimens and Cu_2S film characterization 20
3.3.1. High sulphide environment (exposure #8) 22
3.3.2. Low sulphide environment (exposure #9) 24
3.3.3. Pre-oxidized specimens 25
3.3.4. Weld metal specimens 27
3.4. Results of hydrogen thermal desorption spectroscopy (TDS) 30
3.5. Sulphide and oxide film XRD characterization 36
4. Discussion 38
5. Conclusions 41
References 43
Acknowledgements 45

Summary

Stress corrosion cracking (SCC) and corrosion of copper in sulphide and chloride containing deoxygenated water was studied at 90°C in sulphide concentrations of 0.001 M and 0.00001 M using slow strain rate tensile testing (SSRT) up to 9 % strain. A set of unloaded coupon specimens was simultaneously exposed to the same environments. Several intergranular defects were found in the SSRT specimen exposed to the high sulphide environment, but similar defects were not found in the low sulphide conditions. Only some corrosion on grain boundaries and slip lines was visible. The hydrogen content measurements show an increase in hydrogen uptake of the mechanically loaded SSRT specimens in both conditions when compared to the unloaded coupon specimens and unexposed as-supplied state of the studied oxygen-free phosphorous alloyed copper (Cu-OFP). In the low sulphide environment, the difference between the mechanically loaded specimen and the mechanically unloaded coupon specimens is pronounced, likely because of hydrogen outgassing of the unloaded coupon specimens. This results in hydrogen content of the mechanically unloaded specimens being lower than the as-supplied state. However, it seems that hydrogen uptake of copper is dependent on both the sulphide concentration and the plastic deformation. The highest hydrogen content, on the other hand, was measured in unloaded coupon specimens of friction stir welded (FSW) copper, welded in air without shielding gas, and tested in the high sulphide environment. The air-welded FSW specimens are a special case since the embedded oxide particles in the weld act as local hydrogen trapping sites. It was also found that the oxide particle stringers are selectively attacked in the sulphide solution. A relatively thick air-formed oxide film covers the canisters when deposited, which will transform into a Cu_2S film in the repository conditions. Thus, some of the unloaded coupon specimens were pre-oxidized. It was observed that the conversion of the pre-existing oxide film into a Cu_2S film occurs quickly and the transformation is almost 100 % efficient. The Cu_2S film that formed on the pre-oxidized specimens was very similar to the films formed on all the other copper specimens. In the report, the structure and properties of the Cu_2S film, susceptibility to sulphide-induced SCC, and hydrogen uptake of copper in reducing, anoxic repository conditions are discussed.

Keywords

copper, stress corrosion cracking, sulphide corrosion, sulphide film, hydrogen absorption, friction stir welding

1. Introduction and background

Stress Corrosion Cracking (SCC) of copper in conditions relevant to final repository of spent nuclear fuel is considered possible, but not likely to occur [1]. The key agents known to induce SCC of copper (ammonia, acetate, nitrite) are expected to be present during the aerobic phase of disposal, but not in sufficient amounts to induce SCC. During the long anaerobic phase, sulphide ions (SH^-) in groundwater will be transported to the canister surface by diffusion through the saturated bentonite, which causes sulphidation of the copper and general corrosion on the canister surface. The corrosion rate is limited by the mass transport of sulphide ions through the bentonite buffer [1]. However, before full saturation of the bentonite, the mass transport is less limited, and conditions for sulphide producing microbial activity in the buffer are more favourable.

Indications of sulphide-induced SCC of copper have been reported at a sulphide concentration of 0.01 M [2], which is considerably higher than typically expected in the repository conditions. However, a recent collaboration study between Studsvik Nuclear AB, Sweden, and Aalto University, Finland, involving slow strain rate tensile testing (SSRT) of Cu-OFP in 0.1 M NaCl containing solution with varying content of S^{2-} (added as Na_2S) from 0.001 M to 0.00001 M [3, 4] showed that cracking can occur at sulphide concentration of 0.001 M. This is an order of magnitude lower than the value reported before [2], but still higher than the highest measured sulphide ion concentration in the Swedish planned site for final repository in Forsmark (0.00012 M) [5]. The specimens were studied post-testing for hydrogen uptake. The hydrogen content of copper increased from 0.5 wt.ppm to 1.2 wt.ppm during the short term SSRT testing of two weeks. This may be compared to the maximum allowed hydrogen content of copper in the KBS-3 concept of 0.6 wt.ppm [6]. It should be noted that the hydrogen limit defined in the KBS-3 concept is somewhat arbitrary and has no clear connection to any onset of a degradation process. However, the study [3, 4] suggests that SCC cracking of copper in reducing, anoxic sulphide containing environment may involve hydrogen uptake in the copper metal, and that the SCC mechanism may be related to the hydrogen absorption. In all studied conditions, surface defects, not positively attributed to SCC (except for the highest sulphide concentration), were present. The fact that SCC occurred at sulphide ion concentrations close to the expected Forsmark values makes studying sulphide-induced SCC of copper in reducing, anoxic repository conditions important.

The opening of grain boundaries in sulphide-induced SCC of copper may be compared to opening of grain boundaries and hydrogen-enhanced creep of Cu-OFP [7] in electrolytic hydrogen charging. Micro-voids form on the grain boundaries, which are positioned along maximum shear, indicating a process of accommodating the shear stress component, e.g., by grain boundary sliding [7]. It is possible that a similar mechanism is operational in the SCC environment since hydrogen uptake was observed. On the other hand, a simulation study on hydrogen effects on void nucleation in copper shows that hydrogen stabilizes divacancies and promotes vacancy cluster formation [8]. Hydrogen prevents the collapse of large vacancy clusters. Impurities and alloying elements of copper such as O, P, S, and Ag contribute to void formation by capturing vacancies [8].

The implications of SCC occurring in the repository could be severe, risking the release of radioactive substances. To estimate the risk of sulphide-induced SCC of copper in detail, longer exposures and lower strain rates are necessary when compared to the previous laboratory testing [3, 4]. The SCC mechanism of Cu-OFP in the repository conditions is still unknown. Therefore, additional exposures were conducted to study especially the ox-

ide/sulphide film transformation, structure and properties of the Cu_2S film, SCC, and hydrogen uptake of copper under reducing, anoxic repository conditions. The results deepen the understanding of these phenomena in conditions relevant for final disposal of spent nuclear fuel.

2. Experimental work

2.1. Test materials and specimens

The material used in the SSRT tests was phosphorous-alloyed oxygen-free copper (Cu-OFP) cut from the top part of a canister lid [3], delivered originally by the Swedish Nuclear Fuel and Waste Management Co. (SKB) to Studsvik Nuclear AB through co-operation with the Swedish Radiation Safety Authority (SSM). The same material was used in the earlier studies [3, 4]. The chemical composition is shown in Table 1.

Table 1. Specification of chemical composition of Cu-OFP used in the tests (in wt.ppm, except for Cu).

Cu	O	P	Pb	Bi	As	Sb	Sn	Zn	Mn	Cr	Co	Cd	Fe	Ni	Ag	Se	Te	S
99.99 wt-%	1-2	43-60	<1	<1	<1	1	<0.5	<1	<0.5	<1	<1	<1	<1	2	12	<1	<1	6

The shape of the SSRT specimens was previously determined by finite-element method (FEM) calculations to obtain a desired strain in the gauge section [3]. The maximum strain was 9 % in the narrowest section, allowing a 1.3 mm total elongation. The main dimensions were diameter of ø4.2 mm at the narrowest section, ø8.0 mm at the thick section, and 35 mm length of the tapered section [3]. The tested SSRT specimens, post exposure, are shown in Figure 1 together with the locations of samples cut for hydrogen content measurements by thermal desorption spectroscopy (TDS).

In addition to the SSRT tensile specimens, additional mechanically unloaded coupon specimens were exposed simultaneously to the same sulphide containing environments. The specimens were then studied for sulphidation and hydrogen uptake. The coupon specimens were cut from the as-supplied base material, as well as from two different canister friction stir welds (FSW) provided by the Swedish Nuclear Fuel and Waste Management Co. (SKB), Sweden, and by Posiva Oy, Finland. The first FSW canister weld was welded in air and provided by SKB, and the second one was welded in argon (Ar) shielding gas and provided by Posiva Oy. However, the welding in both cases was performed by SKB. These welds are named 1W (welded in air) and 2W (welded in argon), respectively, when discussing the results. The FSW coupon specimens were cut in such a manner that the processing zone where the oxide particle stringers are located were exposed to the environment to reveal a possible Cu_2O particle sulphidation and consequent penetration along the oxide particle stringers into the weld metal. In addition, some of the unloaded coupon specimens were pre-oxidized using the method of Aaltonen et al. [9] to simulate a thick copper oxide film, which will be present on the canister surfaces at the time of disposal. The size of the coupon specimens was 20×20×2 mm. Naming of the specimens exposed in each exposure are summarized Appendix I.

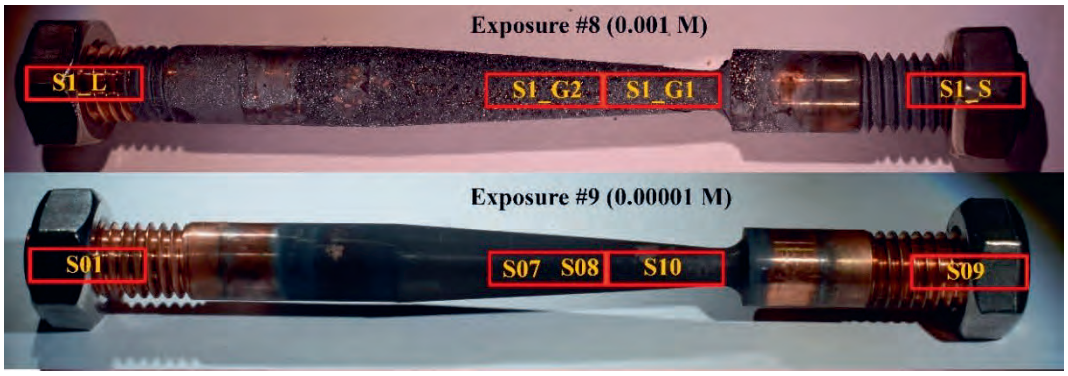

Figure 1. SSRT specimen #8 (top) and #9 (bottom) after testing. Locations and naming of TDS samples are marked with red rectangles and yellow text.

2.2. Autoclave exposures

The autoclave apparatus [3] of Studsvik was used to perform two exposures (#8 and #9) in controlled environment with lower strain rate than in the previous testing [3, 4]. In each exposure, the tensile specimen and 12 copper coupons cut from the lid base material and the FSW weld metals were simultaneously exposed. A special holder made of PTFE was constructed for these coupon specimens. The autoclave loop was used to control the temperature at 90°C and the test solution at the desired concentration (see Table 2). The chemistry of the solution was controlled by addition of a dosage solution containing 0.1 M NaCl and the desired amount of Na_2S to the main flow. A second dosage flow containing Na_2HPO_4 and NaH_2PO_4 was used to control the pH of the solution at 7.2. Several parameters were monitored during testing, including the electrochemical corrosion potential (ECP) of the specimens to ensure a stable deoxygenated environment. The ECPs of both exposures for the whole duration of the test are shown in Figure 2, while all exposure data is presented in Appendix II. The ECP of specimens #8 and #9 were -720 mV and -370 mV vs the standard hydrogen electrode (SHE), respectively, which indicates that a reducing, anoxic condition existed throughout the full exposures.

Table 2. Target test parameters for the two exposures in the autoclave.

Parameter		Target value
Temperature		90°C
Cl^- (added as NaCl)		0.1 M
S^{2-} (added as Na_2S)	Exposure #8	1×10^{-3} M
	Exposure #9	1×10^{-5} M
Autoclave flow rate		1 l/h
Maximum strain		9 %
Test time		4 weeks

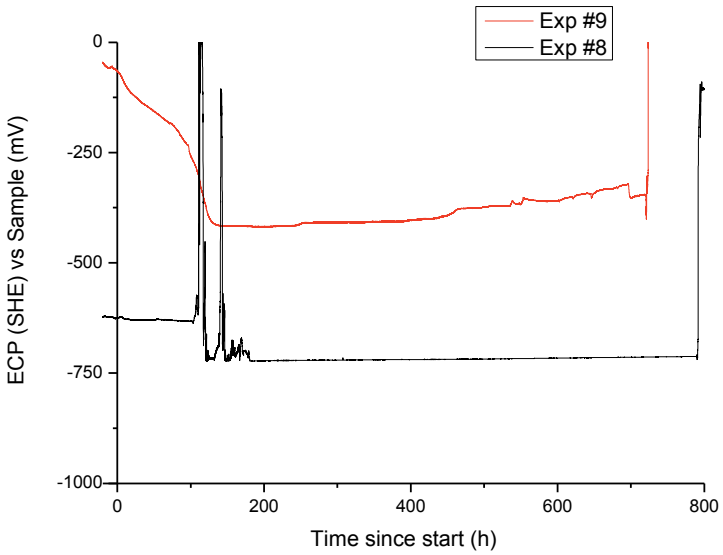

Figure 2. ECPs of exposures #8 and #9.

Each exposure experienced some minor incidents that needs special consideration:

- Approximately four days into exposure #8 at two separate occasions, the autoclave experienced loss of main pump flow, followed by loss of heating. The first occasion lasted for approximately ten hours, during which the autoclave cooled to ambient conditions. Deformation of the SSRT specimen was at this point still elastic. The second occasion occurred shortly after the first one, while no additional strain was applied to the SSRT specimen. Following this, the main pump was replaced, and the exposure saw no more incidents.
- Right before the end of exposure #9, the dosage solution containing the buffer solution was halted, meaning that for the last day only the chloride/sulphide solution was added to the main flow.

As the first incident occurred during the elastic phase of deformation and the second occurred close to the end of the exposure, the two incidents were deemed not to have any critical impact on the quality of the results.

2.3. Specimen examination

Following the exposures, both the SSRT and coupon specimens were removed from the autoclave and transported from Studsvik AB to Aalto University where the analytical observations of the Cu_2S films and surface defects, as well as the hydrogen measurements were performed. Following the exposure, but prior to the examinations, the SSRT specimens were primarily only cleaned by rinsing with ethanol without removal of the Cu_2S films. After initial observation of the SSRT specimens, additional ultrasonic cleaning in ethanol was applied, which removed the Cu_2S films quite easily. The Cu_2S films and surface defects were observed first with optical microscopy and macroscopy, and then by scanning electron microscopy (SEM). The SEM observations were performed with a Zeiss Merlin VP Compact field emission gun SEM (FEG SEM) equipped with a Bruker xFlash 6|30 energy-dispersive spectrometry (EDS) detector. The electron backscatter diffraction (EBSD) measurements were performed with a Zeiss Ultra 55 FEG SEM equipped with

HKL Nordlys II EBSD detector. Specimen preparation for EBSD involved polishing down to ¼ µm diamond paste and vibratory polishing in colloidal silica for at least 48 h to remove deformation from the surfaces. Additional measurements were performed at Helsinki University for some of the coupon specimens with x-ray diffraction (XRD) to study the structure of the Cu_2S films.

2.4. Hydrogen thermal desorption spectroscopy (TDS)

The unloaded reference coupon specimens and SSRT specimens were studied for hydrogen uptake with thermal desorption spectroscopy (TDS) at Aalto University. The apparatus is based on a precise mass-spectrometry measurement of gas partial pressure in ultra-high vacuum (UHV) chamber, equipped with a vacuum friendly internal furnace. It allows the measurement of hydrogen desorption in temperature range of 20 to 1200°C with a controlled heating rate between 1 and 10°C/min. Normal vacuum in the UHV chamber is about 5×10^{-9} mbar, providing the possibility to monitor hydrogen in copper at concentration down to 0.02 wt.ppm. After conversion of the measured partial pressures of hydrogen to desorption rate (in at.ppm or wt.ppm per second), the hydrogen concentration is calculated as the area under the measured TDS curve.

Samples for the TDS measurements were cut with electro discharge machining (EDM) from different parts of the tapered SSRT specimens (see Figure 1) and mechanically from the copper coupon specimens after exposure to the sulphide-containing environments. The TDS samples cut from the SSRT specimens were taken from the threaded parts, subjected to the minimum load, and from the narrow gauge-section, subjected to the maximum load. All the different types of exposed coupon specimens were measured for hydrogen uptake, meaning the base material, the two different FSW welds, and the pre-oxidized coupons. Additionally, reference TDS samples were cut from the as-supplied base material and from the air-welded FSW weld.

In order to remove the surface layer affected by the EDM cutting or mechanical cutting, the samples for TDS were mechanically ground to size of about 0.9×3.8×10.0 mm, finishing with 2000 grit silicon carbide (SiC) paper. Some TDS specimens, cut from the copper coupons, were ground only from one side leaving the Cu_2S layer on the other side unaffected, which provides conditions for estimation of hydrogen distribution in the Cu_2S film and copper substrate. Hydrogen uptake in the Cu_2S film itself was also measured from Cu_2S powder removed from one of the copper coupon specimens, which was exposed to the high sulphide environment. Just before TDS measurement, the samples (except for the powder specimen) were cleaned in acetone in an ultrasonic bath for one minute and dried in pure helium gas flow.

2.5. X-ray diffraction (XRD)

The structure of the films formed on the copper surface was studied with x-ray diffraction (XRD) analysis. The x-ray diffraction measurements were performed at Helsinki University with PANalytical X'Pert Pro MPD in grazing incidence geometry (GIXRD) using x-ray mirror and parallel plate collimator for the parallel beam optics, and 1° constant incident angle. One of the films (from coupon specimen B3_HS) was removed from the copper substrate, ground to fine powder, and then measured in Bragg-Brentano geometry using programmable incident and anti-scatter slits and PIXcel 1D detector.

3. Results

3.1. SSRT specimen exposed to the high sulphide environment (exposure #8)

3.1.1. Optical and SEM observations

SSRT specimen #8 was tested in 0.001 M sulphide solution at 90°C together with the coupon specimens. The general appearance of the coupon specimens and the tensile specimen after testing is shown in Figure 3. A thick, multi-layer Cu_2S film formed on the SSRT specimen, as well as on the coupon specimens. The films are different in their structure since the film on the SSRT specimen was repeatedly detached from the surface during deformation of the specimen, whereas the film on the unloaded coupon specimens did not detach as easily. Figure 4 shows macrographs of the Cu_2S film formed on the tensile specimen. The films are very brittle, and thus crack easily already during tensile testing.

a) b)

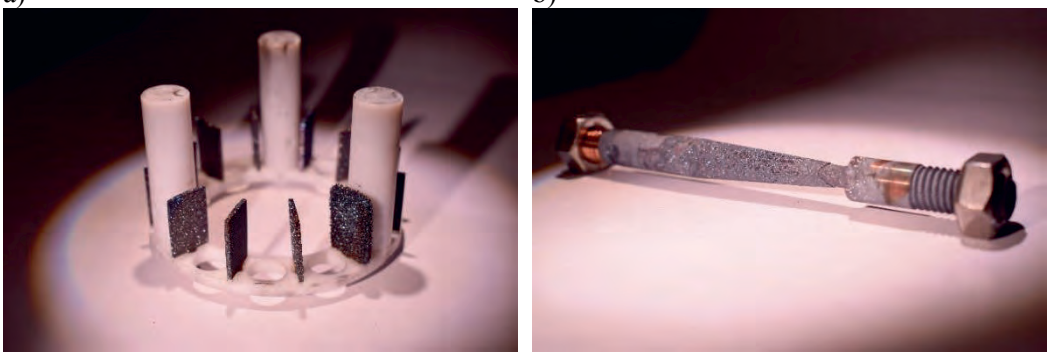

Figure 3. General view of a) coupon specimens and b) SSRT specimen #8 after testing.

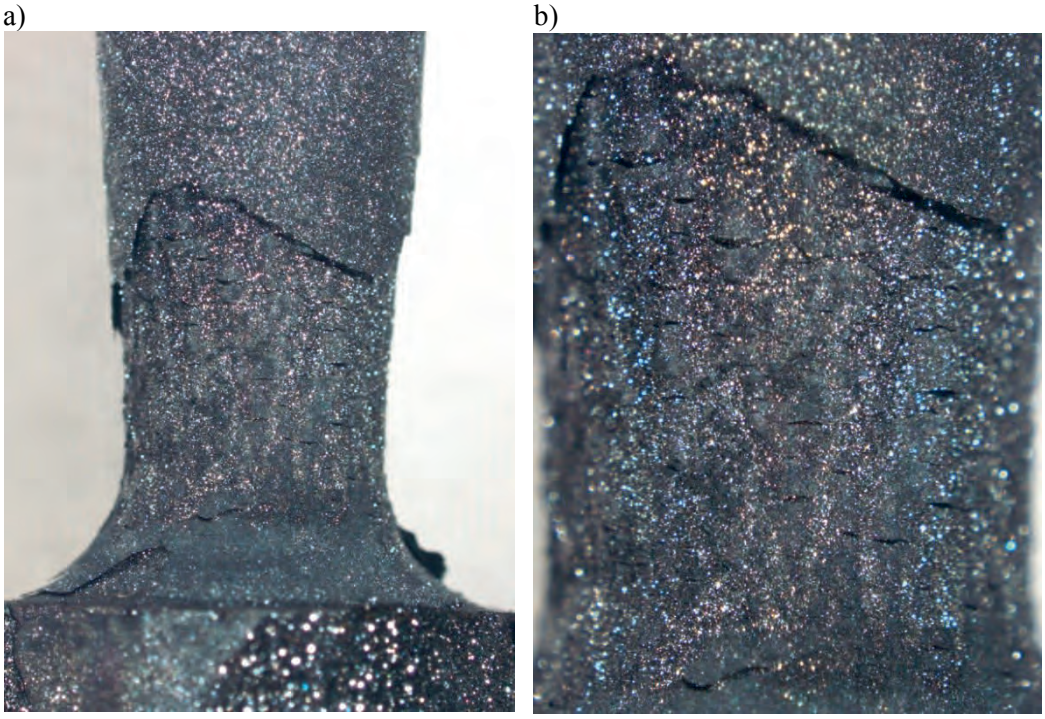

Figure 4. Macrographs of specimen #8 after testing in the high sulphide environment.

The film structures and compositions were examined in detail using scanning electron microscopy (SEM) and energy dispersive x-ray spectroscopy (EDS). The SEM images in Figure 5 show how the different layers of the Cu_2S film crack and detach from the copper surface. It is evident from the wavy appearance of the outer cracked Cu_2S film that the films detach due to deformation of the tensile specimen. Similar wavy appearance was not observed on the unloaded coupon specimens. However, the volume of the Cu_2S crystals is larger than the volume of the copper substrate, which may also result in a tendency of the Cu_2S film to detach easily.

There are at least three Cu_2S film layers, with different crystal morphologies, formed on the SSRT specimen. As the Cu_2S film detaches from the copper surface, a new film forms underneath the detached one. The Cu_2S crystals grow directly from the copper surface. The crystals were confirmed by EDS to contain Cu and S, meaning that they are most likely Cu_2S crystals, later confirmed by the XRD measurements. The surface beneath the crystals, visible for example in Figure 5 d) was confirmed by EDS to be Cu.

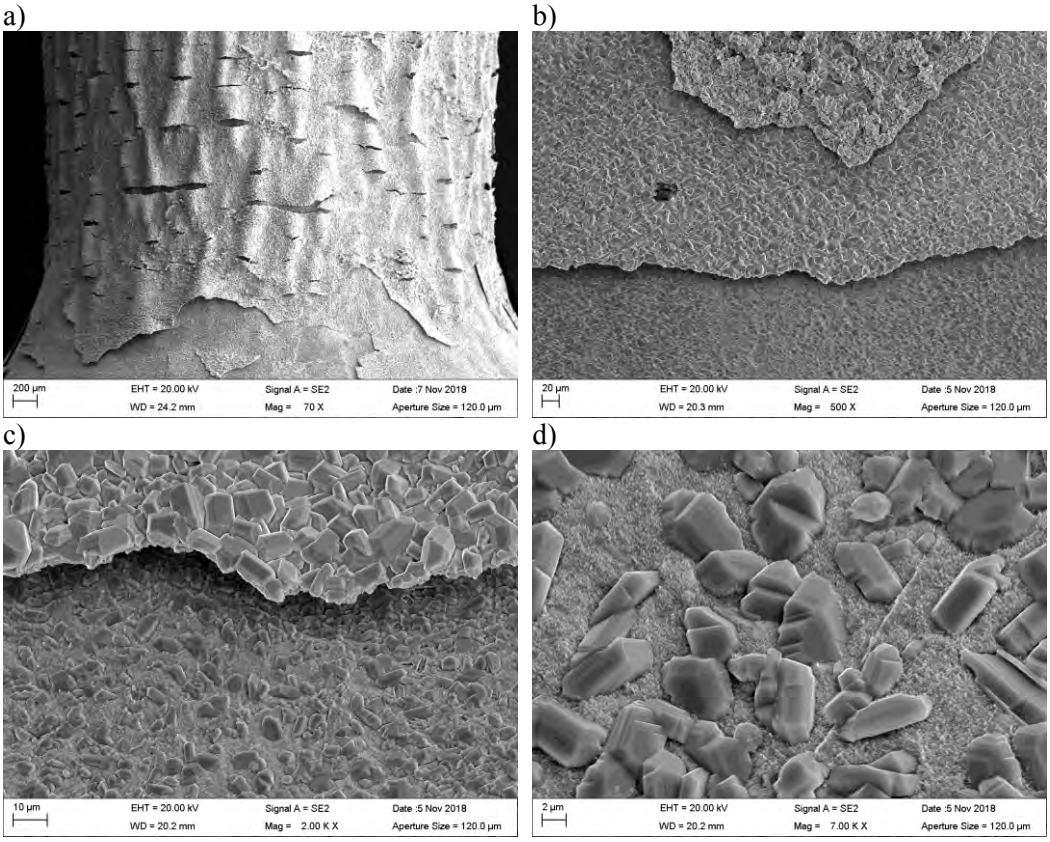

Figure 5. a) General view of SSRT specimen #8. b) Several Cu_2S film layers formed. c) The films detach from the copper surface due to deformation of the specimen. d) The Cu_2S crystals grow directly from the Cu surface.

Figure 6 shows details of the Cu_2S films. The films crack perpendicular to the loading direction, as shown in Figure 6 a) and b). The cracking has revealed another layer of Cu_2S film beneath the top film with a different crystal morphology. The outer detached film has much smaller crystal size, and the size of the crystals varies greatly, whereas the inner (also detached) film has a more consistent grain size and larger crystals. The two morphologies are shown in greater detail ion Figures 6 c) and d). Side-view of the inner detached Cu_2S film is shown in Figure 7. A single layer of Cu_2S crystals has formed and it was detached from the copper surface. Cracking of the film has occurred intergranularly. Since the film is very brittle, the crystals are most likely held in place partly by mechanical locking.

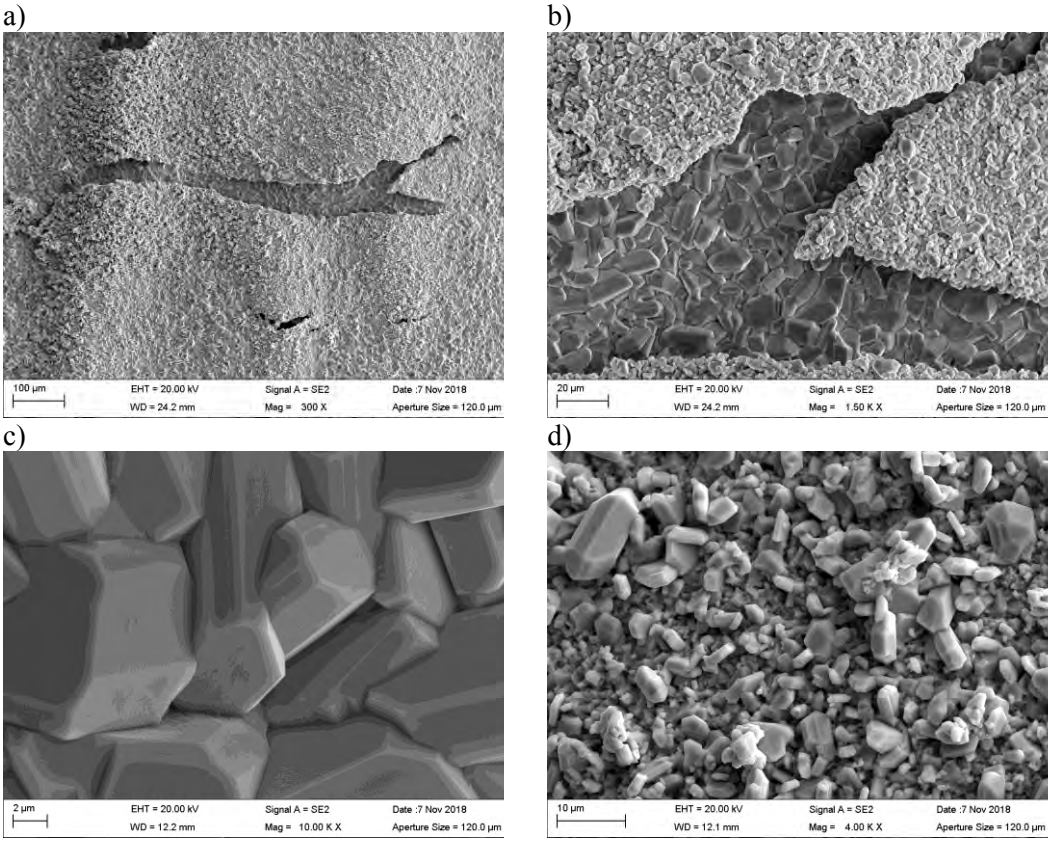

Figure 6. a) The Cu_2S films crack perpendicular to the loading direction. b) Different layers of films have different crystal morphologies. c) The inner (but still detached) film has larger crystals and the size of the crystals does not vary much. d) The outer film has smaller crystals and their size varies more.

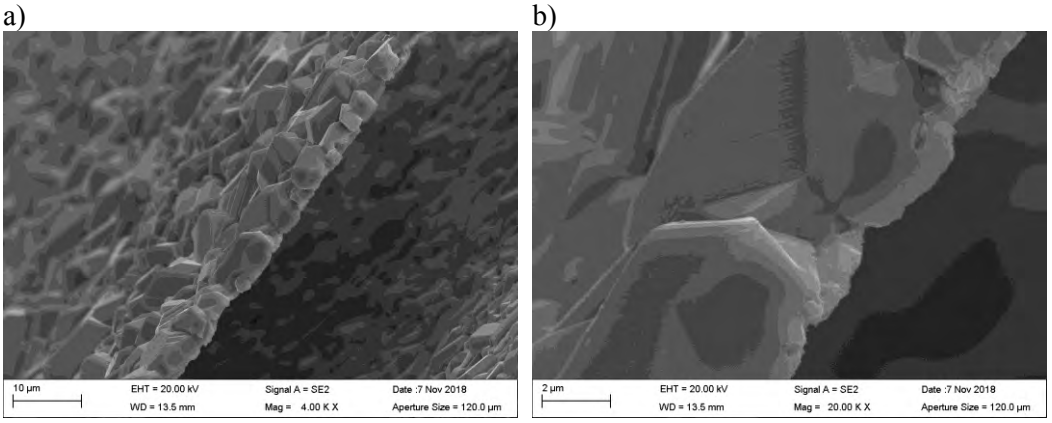

Figure 7. Side view of the inner detached Cu_2S film.

Figure 8 shows details of the Cu_2S crystal growth on the Cu surface. The crystals grow directly from the copper surface, and therefore form a roughened copper surface when the Cu_2S film is removed. No pitting corrosion was found. However, observation of the Cu surface beneath the Cu_2S films revealed the existence of several surface defects resembling

the cracking of grain boundaries found in [3, 4]. These surface defects, shown in Figure 9, form underneath the Cu_2S film, and the Cu_2S crystal growth is also observed inside the defects.

After initial observations, the Cu_2S films were removed by ultrasonic cleaning. This revealed more surface defects underneath. Some of them are shown in Figure 10. The Cu_2S crystals grow inside the open defects, but in many cases the cracks are not completely filled with the corrosion products, allowing the transportation of corrosion agents in the solution inside the defects. In many locations, small pitting-like corrosion attack, as shown in Figure 11, was present on the grain boundaries. These corrosion defects may later form larger defects on the grain boundaries by joining as shown in Figure 10 d). Similar defects were not found in the unloaded coupon specimens.

a) b)

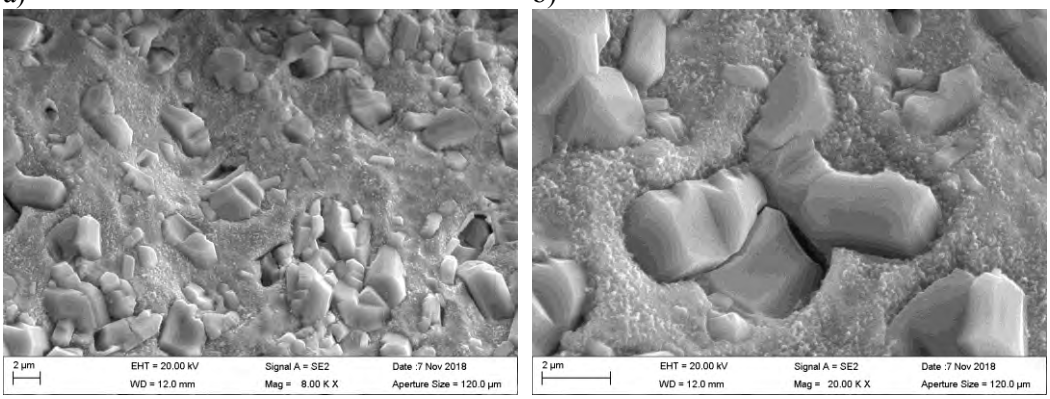

Figure 8. Cu_2S crystals grow directly from the Cu surface.

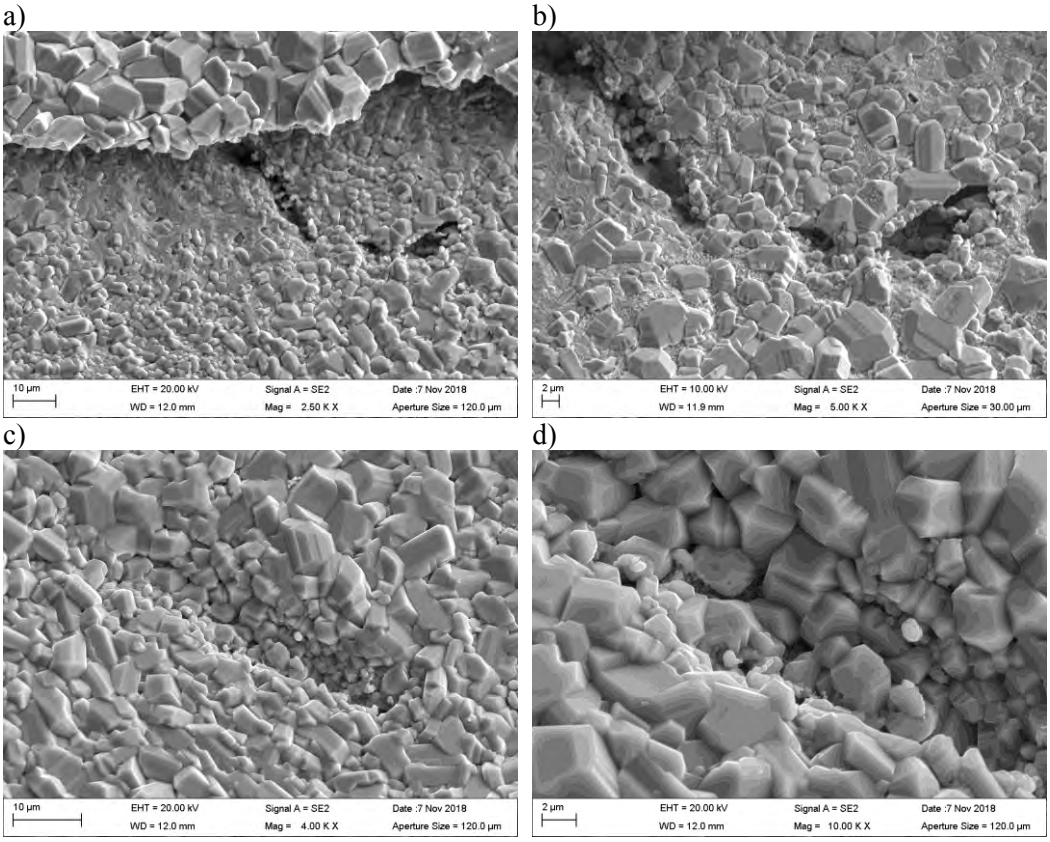

Figure 9. a) Surface defects form on the Cu surface underneath the Cu_2S film, b) the defects forming on grain boundaries, and c, d) the Cu_2S crystals growing inside the defects.

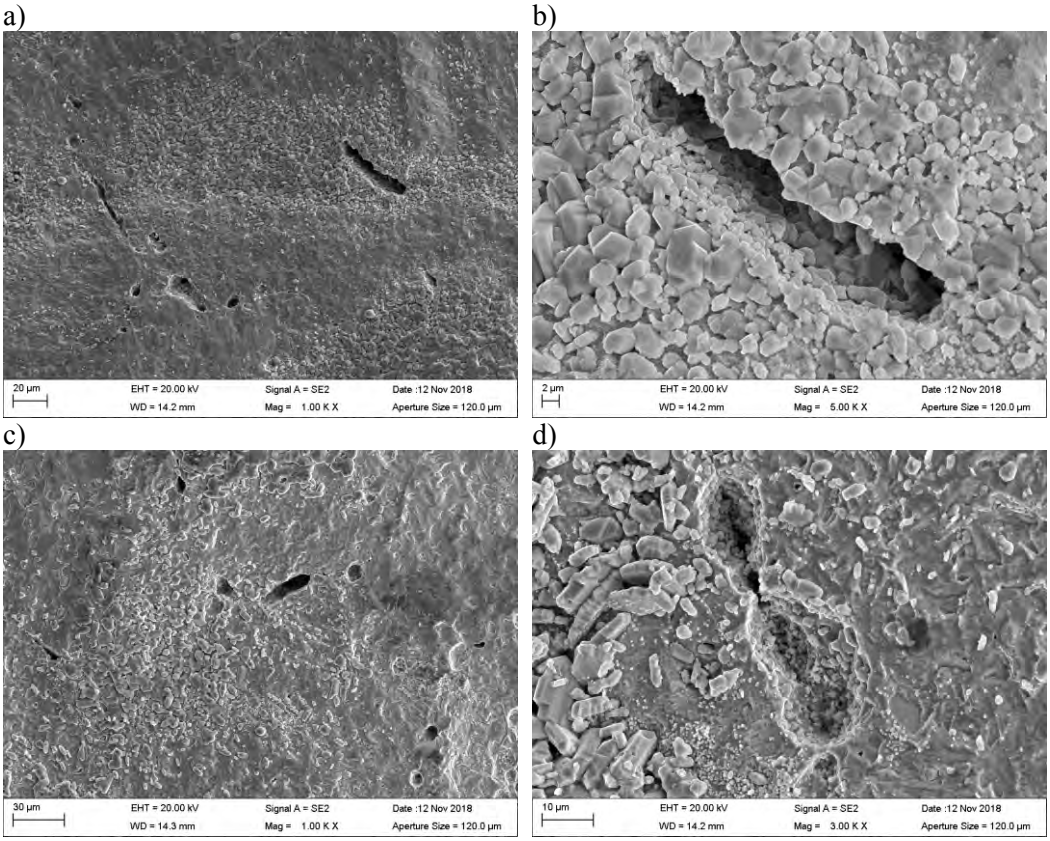

Figure 10. Surface defects underneath the Cu_2S film were revealed by film removal with ultrasonic cleaning.

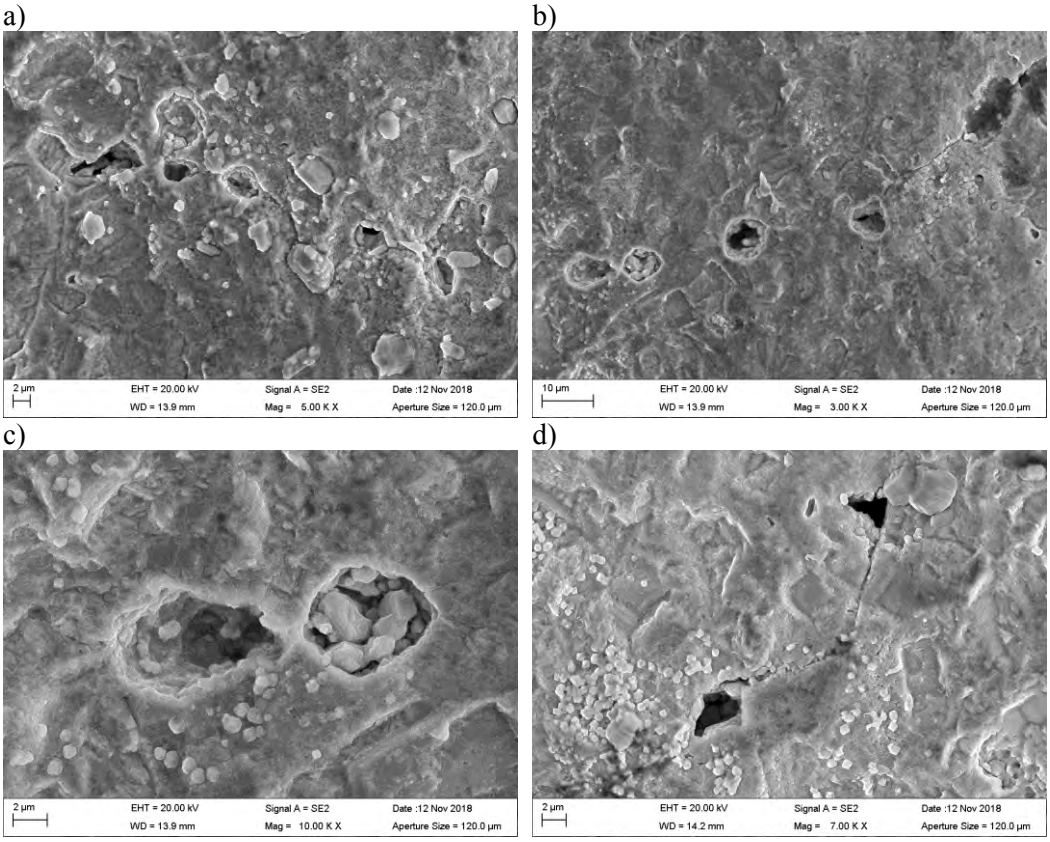

Figure 11. Small pitting-like corrosion attack forms on the grain boundaries.

3.1.2. EBSD of the surface defects

The locations of the largest surface defects in specimen #8 were determined and measured by SEM observations, and the tensile specimen was cut in half by EDM from that location. The cross-section was then carefully polished for EBSD to reveal the small surface defects. As a result, several surface defects were found in the same cross-section. Some of them are shown in Figure 12. The inverse pole figure (IPF) colour key for the maps is shown in Figure 13, which may be used to interpret the orientation of the Cu grains in the EBSD maps (although IPF colouring loses some of the information of the orientation).

The EBSD maps reveal that the defects form on the grain boundaries of copper, most preferably on random high-angle grain boundaries indicated by black coloured lines between the grains. Red coloured lines indicate twin grain boundaries. However, in one instance, shown in Figures 12 a) and b), the defect formed on a thin twinned grain following the path of two parallel twin boundaries. All the defects found in this specimen were rather small with lengths of about 10-15 µm. No deep cracks, as observed in [3, 4] in the same conditions, were found. The length of the longest crack in [3, 4] was about 70 µm.

a)

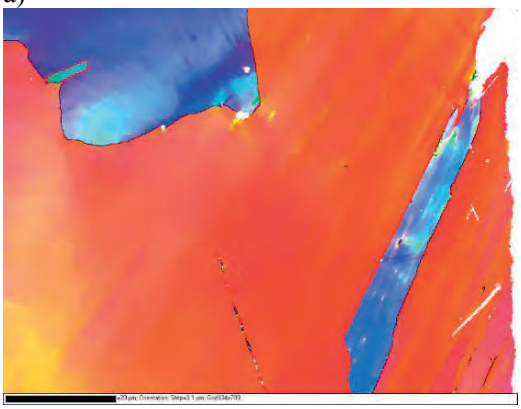

b)

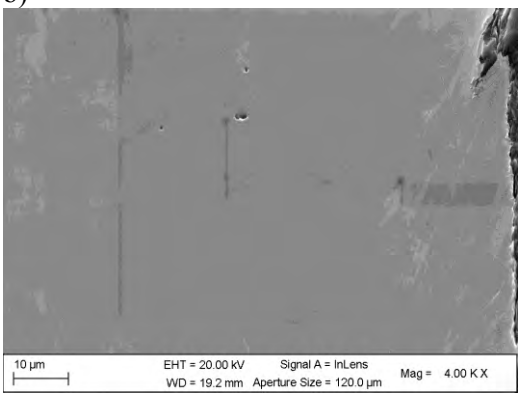
10 µm
EHT = 20.00 kV
WD = 19.2 mm
Signal A = InLens
Aperture Size = 120.0 µm
Mag = 4.00 K X

c)

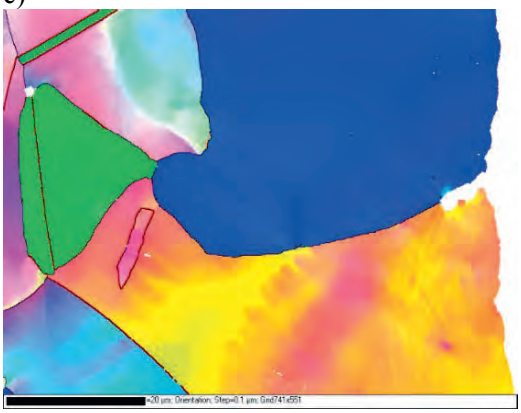

d)

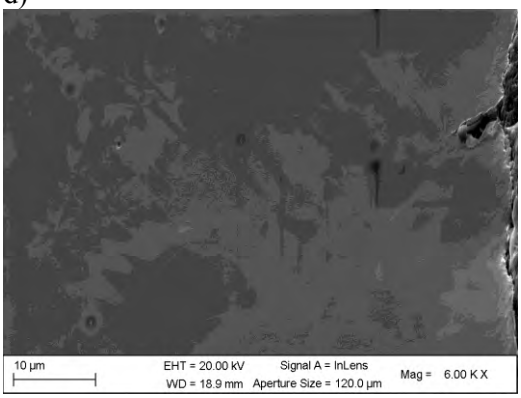
10 µm
EHT = 20.00 kV
WD = 18.9 mm
Signal A = InLens
Aperture Size = 120.0 µm
Mag = 6.00 K X

e)

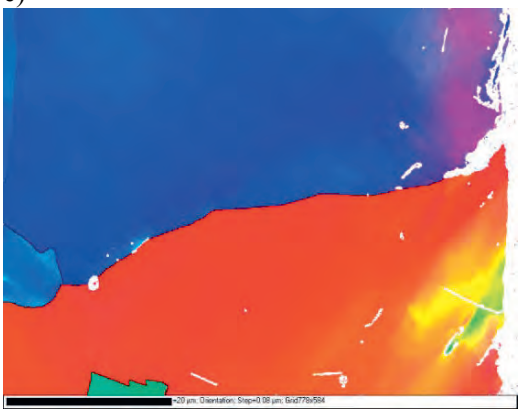

f)

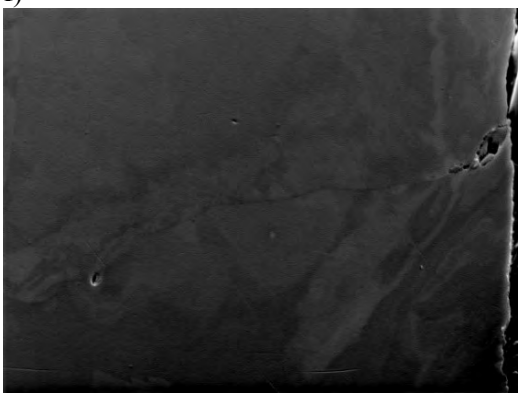

g)

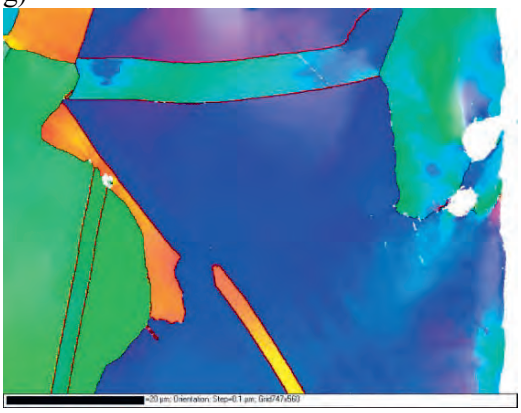

h)

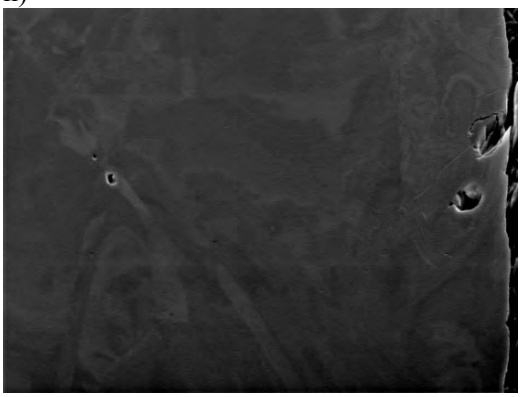

Figure 12. IPF coloured EBSD maps (on the left) and cross-section images (on the right) of several surface defects found in SSRT specimen #8. In the EBSD maps, white is non-indexed data points, black lines represent random high-angle grain boundaries, and red lines represent twin grain boundaries. The length of the black scale bar in the EBSD maps is 20 µm. The orientation of the Cu grains may be interpreted by using the colour key shown in Figure 13.

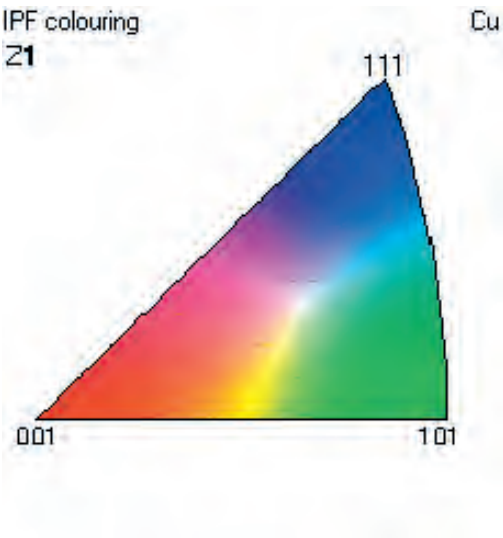

Figure 13. Inverse pole figure (IPF) colour key of the EBSD maps in z-direction.

3.2. SSRT specimen exposed to the low sulphide environment (exposure #9)

3.2.1. Optical and SEM observations

Specimen #9 was subjected to the low sulphide concentration of 0.00001 M, which is an order of magnitude lower than the highest measured sulphide concentration in the Forsmark groundwater. Figure 14 shows the general appearance of the coupon specimens and the tensile specimen #9 after testing. Figure 15 shows the surface of the tensile specimen examined with an optical macroscope. The appearance of the Cu_2S film is very different from specimen #8 and much thinner, although still very brittle and very easily removed.

SEM observations prior to ultrasonic cleaning revealed a thin wavy Cu_2S film with smooth base layer and crystal-like features forming on top of it, as shown in Figure 16. The crystal-like features were easily destroyed by the electron beam of the microscope when subjected to close observation with high magnification, meaning that they are not similar crystals as those observed in specimen #8. It is possible that the crystal-like features formed during the cool-down period of the autoclave at the end of the test or due to the loss of the buffer solution during the last day of exposure when only the chloride/sulphide solution was added to the main flow. The Cu_2S film was also less conductive than the films formed on specimen #8, making close observations with SEM more difficult.

No clear SCC cracks or surface defects were found in this specimen, but many grain boundaries and slip lines were clearly corroded and visible on the surface. Figure 17 shows the corrosion attack on the grain boundaries, as well as cracking of the Cu_2S film when observed prior to ultrasonic cleaning. Figure 18 shows the corroded grain boundaries and clearly visible slip lines, which form due to deformation of the specimen on the copper surface, observed after ultrasonic cleaning.

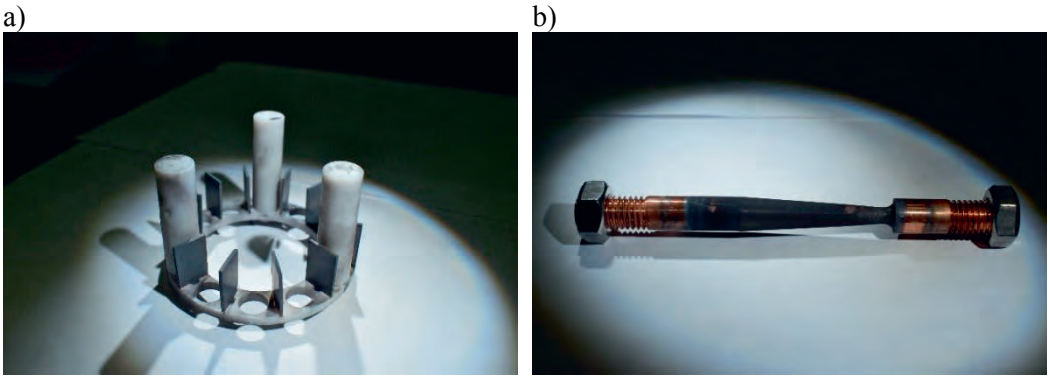

Figure 14. General view of a) coupon specimens and b) SSRT specimen #9 after testing.

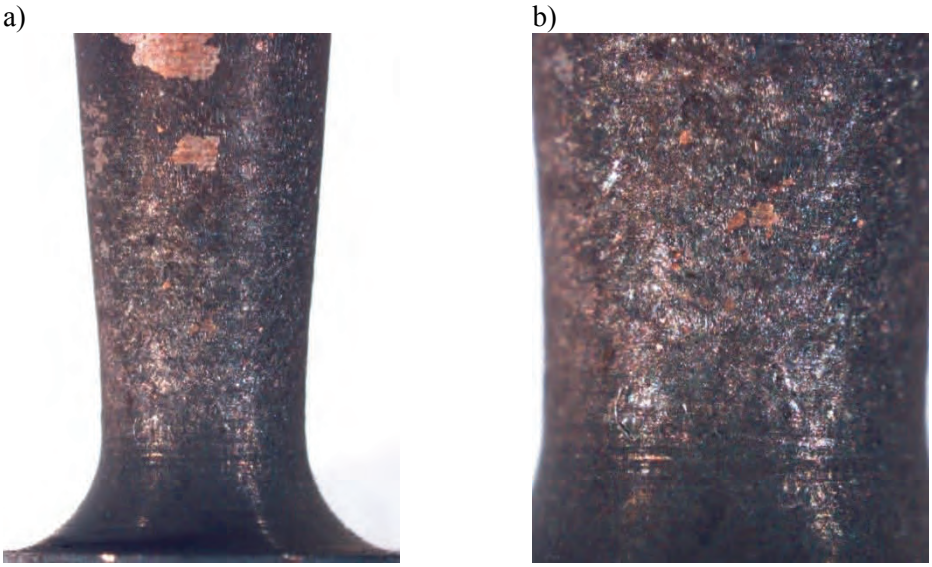

Figure 15. Macrographs of SSRT specimen #9 after testing.

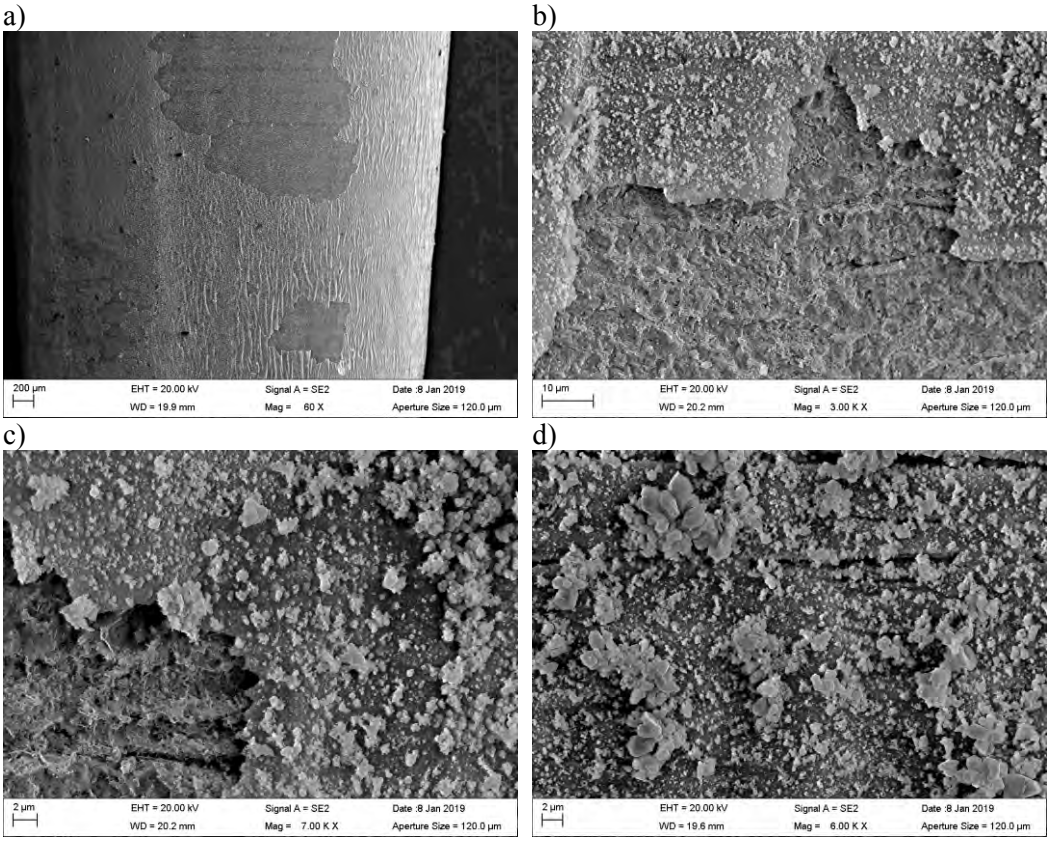

Figure 16. a) General view of specimen #9 prior to ultrasonic cleaning. b) Only one thin and wavy Cu_2S film formed. The film was detached from the Cu surface due to plastic deformation of the specimen. c) The appearance of the film is markedly different from the previous test. d) Small crystal-like features were formed on top of the Cu_2S film.

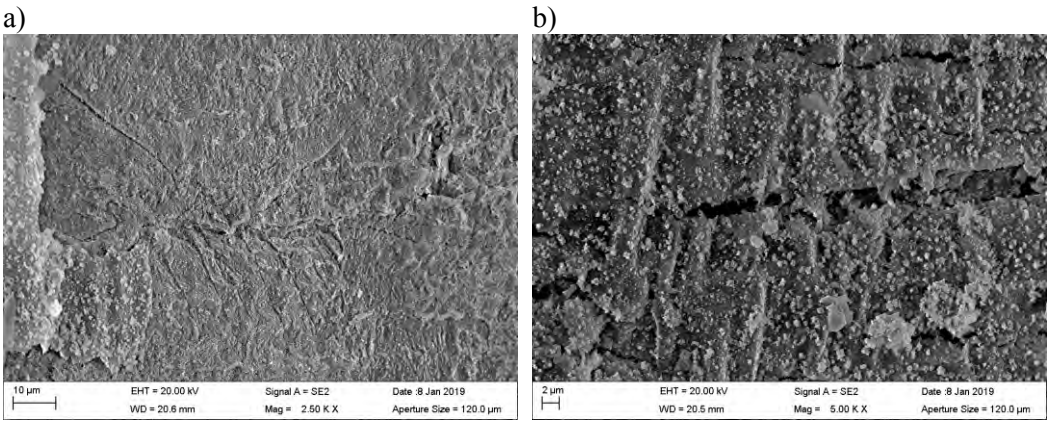

Figure 17. a) Cu surface prior to ultrasonic cleaning with grain boundaries and slip lines visible. b) Cracking of the Cu_2S film.

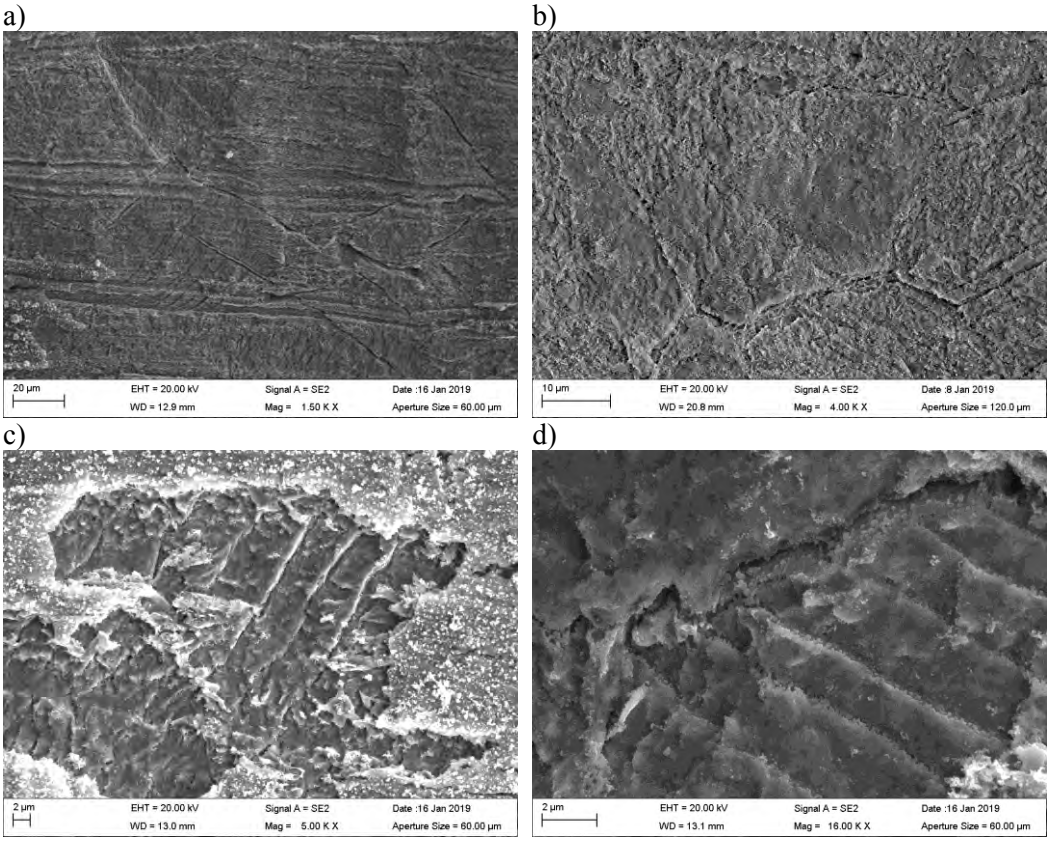

Figure 18. a), b) Cu surface after ultrasonic cleaning with corroded grain boundaries visible. c), d) Clearly visible slip lines on the Cu surface with corrosion attack.

3.3. Unloaded coupon specimens and Cu_2S film characterization

The general appearance of the Cu_2S films formed on the unloaded coupon specimens in the high sulphide (named HS) and low sulphide (named LS) conditions during the four weeks exposure are shown in Figures 19 and 20, respectively. EDS analyses of the films revealed that the corrosion deposits consist of only Cu and S, implying that the corrosion product formed on the copper surface is Cu_2S. This was later confirmed by separate x-ray diffraction (XRD) measurements for the coupon specimens of exposure #8. ECPs of -370 mV and -720 mV vs SHE for the specimens exposed at 0.00001 M and 0.001 M sulphide concentrations, respectively, were rapidly stabilized during the exposure, suggesting also that the corrosion film was Cu_2S, since these values are close to the equilibrium potential for Cu/Cu_2S at these sulphide ion concentrations.

a) b)

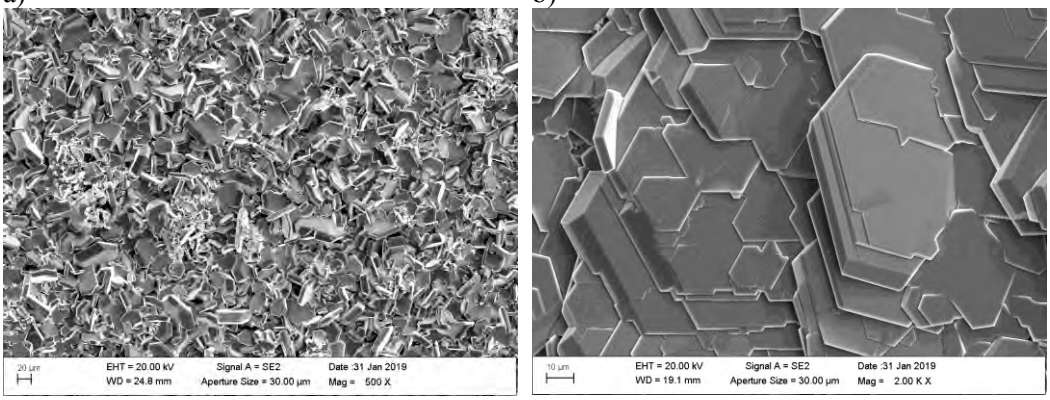

Figure 19. Thick plate-like Cu_2S crystals formed on the Cu coupons during four weeks of exposure in 0.001 M Na_2S solution at 90°C. a) Coupon specimens 1W1_ox_HS and b) 1W2_HS.

a) b)

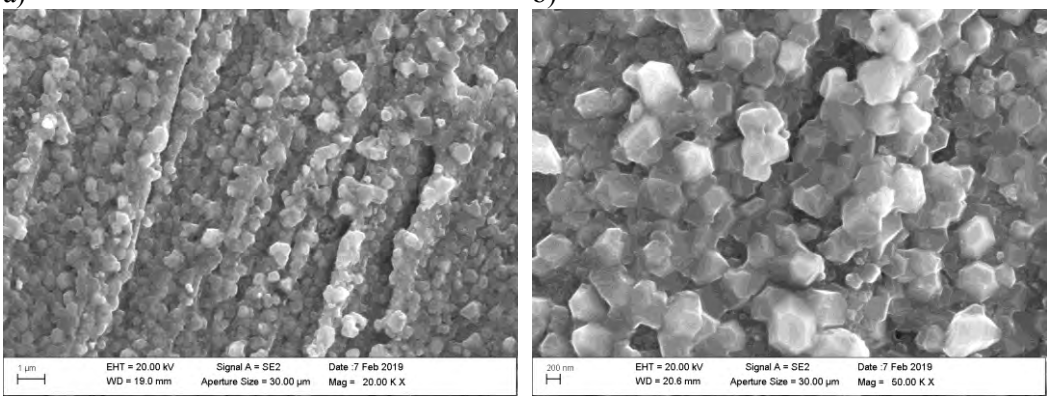

Figure 20. Thin crystalline Cu_2S film formed on the Cu coupon surface during four weeks exposure in 0.00001 M Na_2S solution at 90°C. Coupon specimens a) B5_LS and b) 1W4_LS.

The structure of the films formed on the coupon specimens was found to change from thin (200-400 nm) porous single-layer film to a thick (10-30 µm) more compact, multi-layer film when the sulphide concentration in the solution increased. The two films are shown in Figure 21. These observations confirm that the sulphide concentration in the solution is an important factor influencing the structure and properties of the Cu_2S film.

Three distinct types of Cu_2S films have been reported in the literature, depending on the sulphide concentration [10]. Type I: a thin single-layer, porous film observed at low sulphide concentrations and low sulphide fluxes; Type II: a porous, dual-layer film formed at intermediate and higher sulphide fluxes; and Type III: a passive or at least partially passive film formed at high sulphide concentrations and transport fluxes [10]. In this study, the low sulphide concentration produced a Type I film and the higher sulphide concentration produced a Type II film according to this classification.

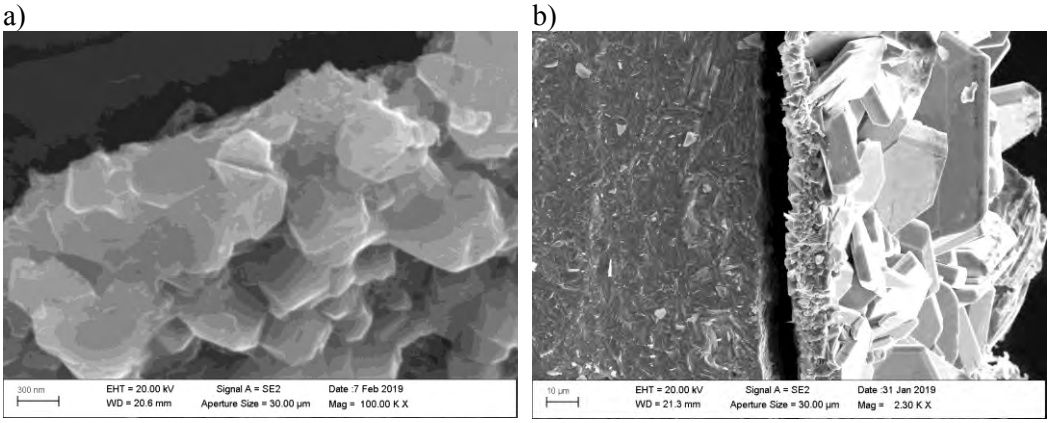

Figure 21. a) Cross-section of thin crystalline Cu_2S film on the Cu coupon after four weeks exposure in 0.00001 M Na_2S solution at 90°C (coupon specimen 1W3_LS). b) Cross-section of thick crystalline Cu_2S film on the Cu coupon after four weeks immersion in 0.001 M Na_2S solution at 90°C (coupon specimen 1W3_HS).

3.3.1. High sulphide environment (exposure #8)

A compact film is formed at the high sulphide concentration. Once the Cu_2S film covers the Cu surface, corrosion proceeds with apparently constant rate by the growth of the film at the Cu_2S/solution interface by Cu^+ transportation through the film, most likely by diffusion along grain boundaries in the crystalline film. The film growth at the Cu_2S/solution interphase can account for the development of the well-defined large crystals of the Type II film. In this case, the Cu_2S crystals are much larger (about 10-20 µm) than for Type I films (about 200 nm). Figure 22 shows the Cu/Cu_2S interface, cross-section of the film, and roughness of the copper surface underneath the Cu_2S film. Three distinct layers can be distinguished in Figure 22 c) based on the grain size and shape. On the left, large columnar grains have grown from the copper surface, on top of this layer equiaxed fine grains have formed, and finally on top of this dual layer, the large plate-like grains have precipitated.

The Cu/Cu_2S interface showed no evidence of localized pitting corrosion. However, Figure 23 clearly shows that the copper surface is markedly roughened when the coherent Cu_2S grains have grown from the copper surface. Crystallographic marks have been left on the copper surface, which match exactly with the size of the crystals in the inner layer of the Cu_2S film. Even though grain boundaries can be discerned from the Cu surface, no marked intergranular corrosion has occurred in the unloaded coupon specimens. This is consistent with the presence of a uniformly distributed porous outer layer and confirms that localized anodic dissolution did not occur (no pitting locations or pitting at grain boundaries), including locations where large pores may have been present in the film.

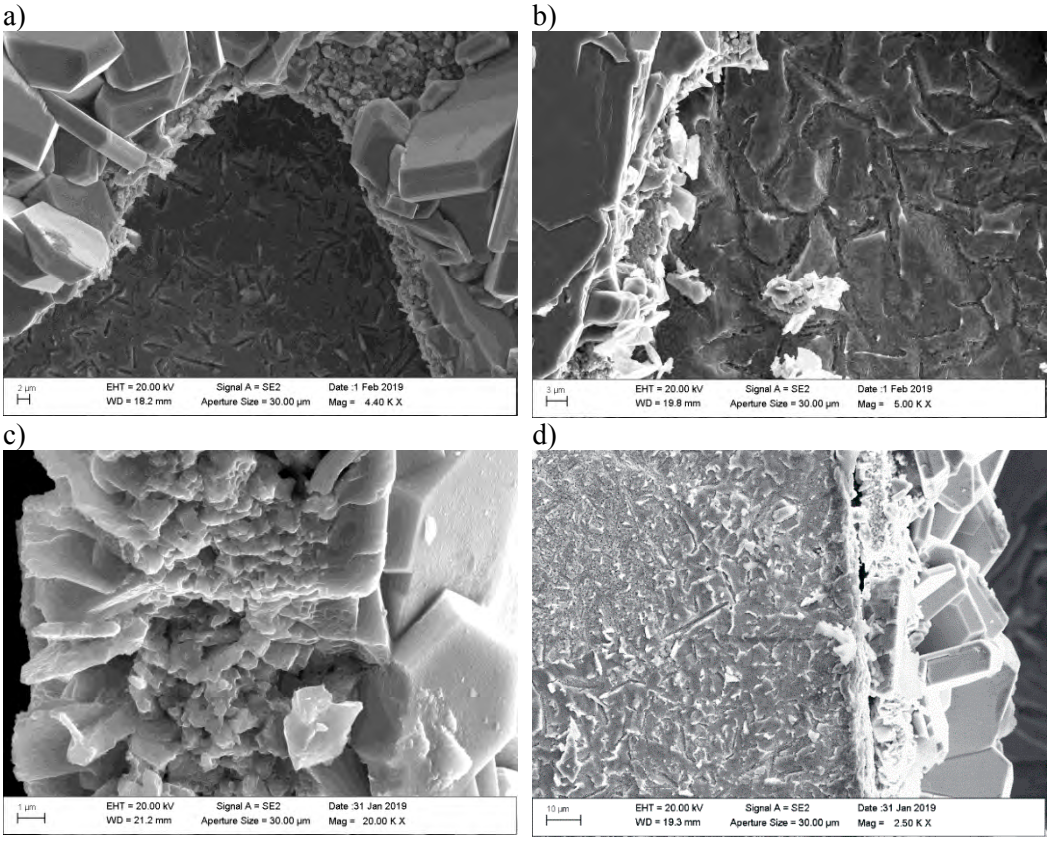

Figure 22. a) Thick Cu_2S film and the underlying corroded Cu surface in coupon specimen B2_ox_HS. b) Similar surface in coupon specimen B3_HS. c) Cross-section of a detached thick crystalline Cu_2S film formed on coupon specimen 1W3_HS. d) Cross-section of Cu_2S film formed on Cu surface of coupon specimen 1W1_ox_HS.

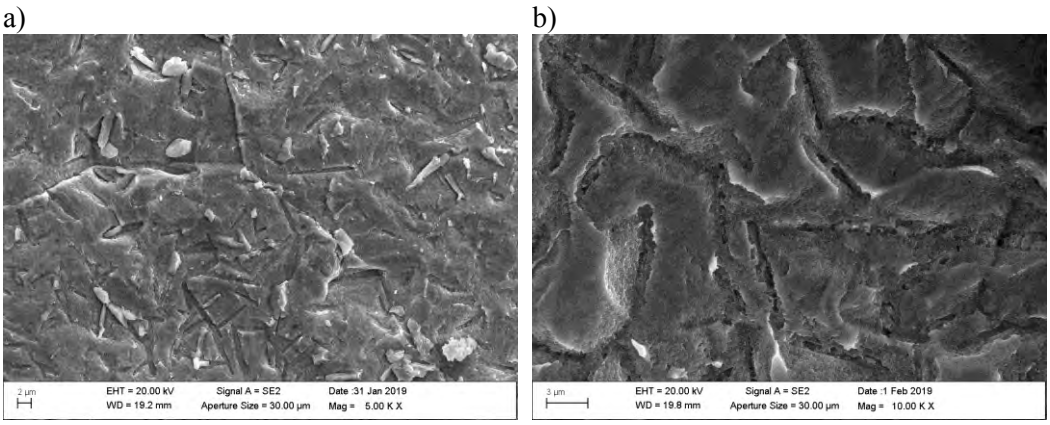

Figure 23. Copper surface underneath the detached thick crystalline Cu_2S film after four weeks exposure in 0.001 M Na_2S solution at 90°C. Coupon specimens a) 2W1_ox_HS and b) B3_HS.

The growth of the coherent Cu_2S film at the Cu/Cu_2S interphase may be limited by the build-up of an interfacial stress leading to film fracture. The Pilling-Bedworth (P-B) ratio for Cu_2S on copper is 2, whereas the ratio for Cu_2O on copper is 1.68. In general, if the P-

B ratio is greater than 1, compressive stresses form in the film, and if the ratio is greater than 2 the surface film is non-protective and may crack and flake off continuously exposing the metal surface [11]. Film growth at the film/solution interphase does not cause a build-up of interfacial stresses, and growth of the outer Cu_2S layer can continue unimpeded at a rate at least partially controlled by sulphide ion (SH^-) diffusion to the film/solution interface. Most of the surface is covered with a relatively uniform deposit. Separation of the Cu_2S film from the copper substrate confirms that the corroded copper surface is roughened but not pitted. The corrosion damage is, however, non-uniform depending on the local crystal growth rates of the coherent Cu_2S crystals of the inner film layer.

The outer film grows outwards by a mechanism controlled by a combination of Cu^+ diffusion in the film and sulphide ion (SH^-) diffusion in the solution. The film grows out from the copper surface in the form of flat plate-like crystals separated by some open spaces. The film growth process may also be partially controlled by a combination of SH^- diffusion in the bulk solution and $CuCl_2^-$ diffusion in the spaces between the Cu_2S plates [12].

3.3.2. Low sulphide environment (exposure #9)

The corrosion film formed on the unloaded coupons in the low sulphide solution is shown in Figure 24. It is a continuous, single-layer cellular Cu_2S film with a non-uniform thickness of about 200-400 nm. The film consists of well-defined granular crystals of the same size in diameter as the film is in thickness. SEM images of openings in the film, shown in Figure 25, indicate that the Cu/Cu_2S interphase shows very little corrosion attack when compared to the high sulphide conditions. There are no indications of localized corrosion behaviour. The grinding marks are still visible on the copper surface.

Due to the roughness, brittleness, and porosity of the film, it is expected that the corrosion product film is not protective. The film growth process seems to be controlled by SH^- diffusion partially in the bulk of the aqueous solution, as well as partially in the aqueous solution in the pores of the fine cellular Cu_2S film.

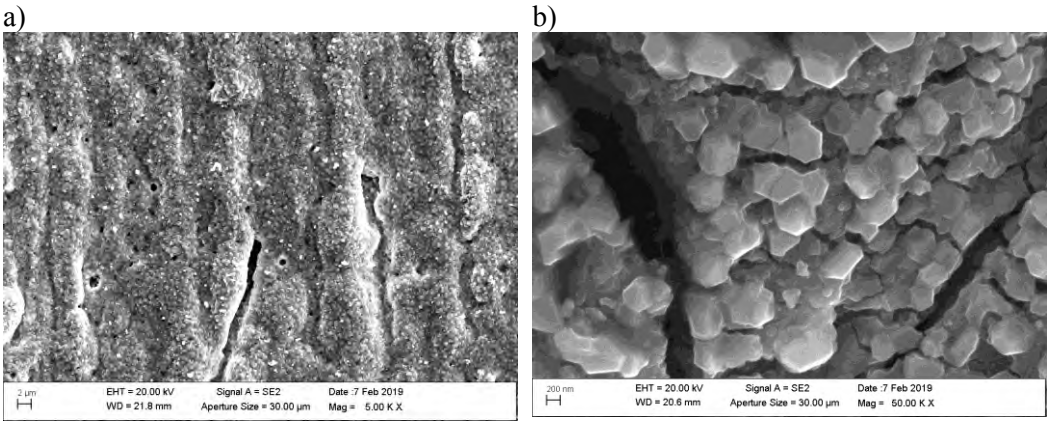

Figure 24. Thin crystalline Cu_2S film on the Cu coupon surface after four weeks exposure in 0.00001 M Na_2S solution at 90°C. Coupon specimens a) 1W1_ox_LS and b) 1W3_LS.

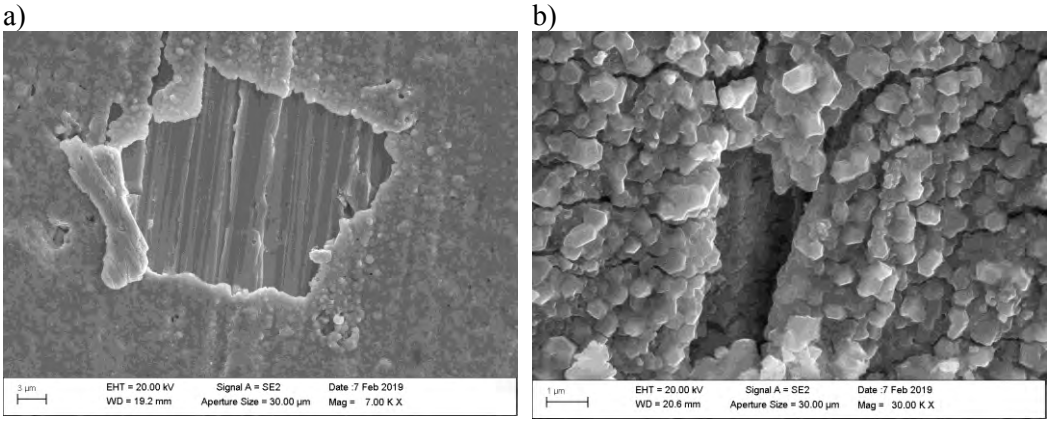

Figure 25. Thin crystalline Cu_2S film on the Cu coupon surface after four weeks exposure in 0.00001 M Na_2S solution at 90°C. Coupon specimens a) 1W1_ox_LS and b) 1W4_LS.

3.3.3. Pre-oxidized specimens

Before exposure, some coupon specimens where pre-oxidized according to the procedure of [9] to study the conversion of Cu_2O film on the copper surface to Cu_2S film in aqueous sulphide solutions. The compositions and morphologies of the oxide films were determined using SEM/EDS and XRD. The appearance of the oxide film before exposure to the sulphide solution is shown in Figure 26.

After four weeks exposure in the high sulphide solution, the Cu_2S film on the specimen surface looks similar to the other specimens, and in general very few traces of the pre-oxidized film are preserved on the surface. Figure 27 shows the structure of a typical Cu_2S film formed on the pre-oxidized specimens after exposure to sulphide solution. When comparing Figure 27 b) to Figure 22 c), which shows a non-pre-oxidized specimen, it can be seen that the inner Cu_2S layer is very similar consisting of the columnar Cu_2S crystals, but the middle layer seems much more porous than in the non-pre-oxidized specimens. The outer precipitated plate-like large Cu_2S crystals are again similar to the unloaded non-pre-oxidized specimen. Locally under the detached Cu_2S film, areas can be found where debris of the pre-oxidized film are still preserved, as shown in Figure 28. EDS analyses of these debris show that they also contain some sulphur, indicating that they have reacted with the sulphide containing solution.

The Cu_2S film formed on the pre-oxidized specimens in the low sulphide solution is thin and contains much porosity, as shown in Figure 29. The shape of the grinding marks is often still visible on the film surface. The Cu_2S crystals are also not as well distinguishable as for the unloaded non-pre-oxidized specimens tested in the same environment. This may be seen, for example, by comparing Figure 25 b) and Figure 29 b), which have the same magnification. Under the film, the copper surface does not seem to be corroded markedly.

The conversion of a Cu_2O film on the copper surface to Cu_2S in aqueous sulphide solutions at both the higher and the lower concentration occurs quickly, and the conversion seems to be almost 100 % efficient. After four weeks exposure to sulphide solutions, the films on specimen surfaces are similar to the non-pre-oxidized specimens. The pre-existing oxide film does not seem to have any major effect on the Cu_2S film forming process.

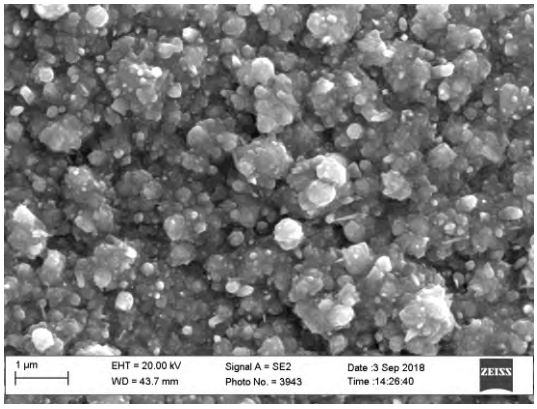

Figure 26. Pre-oxidized Cu surface before exposure to sulphide solution.

a) b)

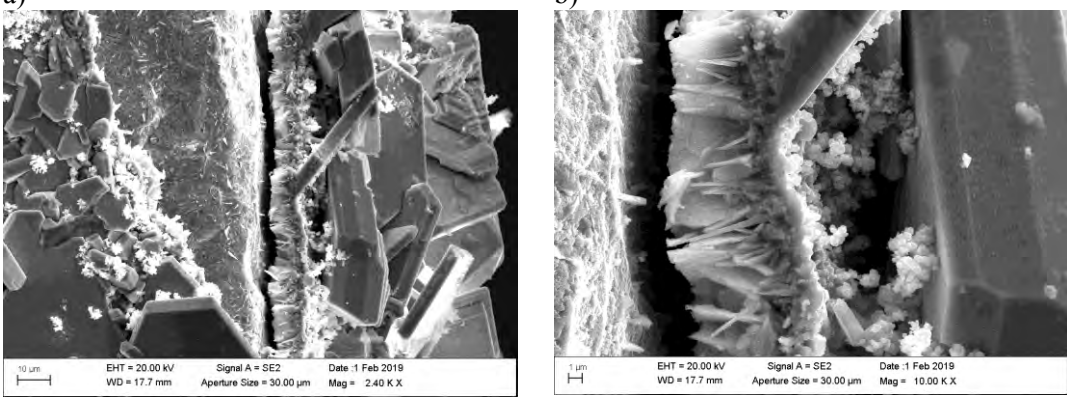

Figure 27. Cross-sections of the Cu_2S film formed on the pre-oxidized copper surface after four weeks exposure in 0.001 M Na_2S solution at 90°C. a), b) Coupon specimen B1_ox_HS.

a) b)

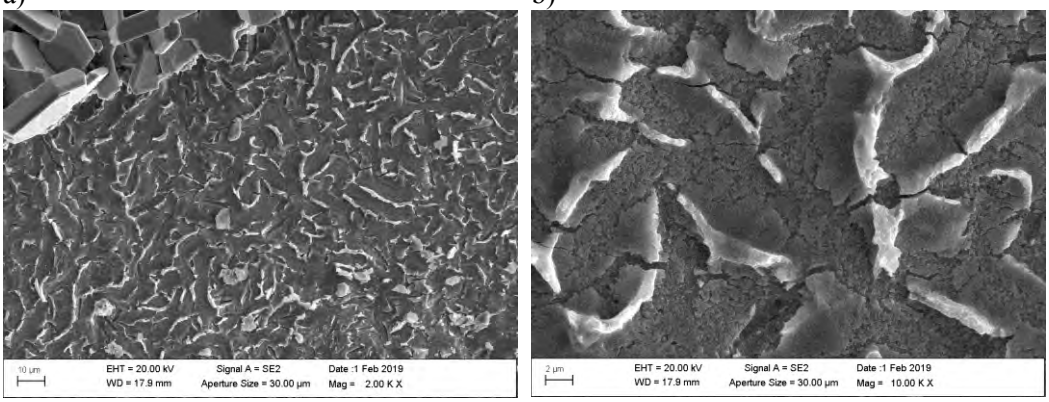

Figure 28. Surface of pre-oxidized specimen under the thick Cu_2S film, showing remnants of the oxide film preserved from the conversion process into Cu_2S film. a), b) Coupon specimen B2_ox_HS.

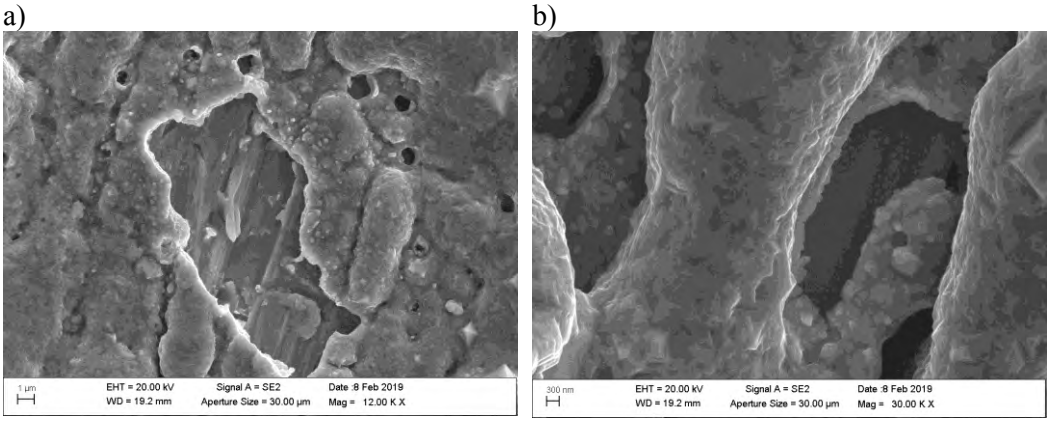

Figure 29. Porosity in the Cu_2S film formed on the pre-oxidized specimen B2_ox_LS during four weeks exposure to 0.00001 M Na_2S solution at 90°C.

3.3.4. Weld metal specimens

FSW weld metal specimens representing both welding in air, named 1W(n), and welding in Ar shielding gas, named 2W(n), where (n) represents the number of the specimen, were exposed in the test solutions simultaneously with the tensile specimen and the other coupon specimens. In general, the Cu_2S film appearance is similar to the films formed on the base material. However, weld metal specimens showed some interesting features that were not present in the base material. Figure 30 a) shows an opening in the Cu_2S film, formed on the air-welded specimen, revealing that the oxide stringers [13] in the weld metal were attacked and sulphidised under the Cu_2S film. In Figures 30 b) and c), opening and depth of the attacked oxide stringers in the weld metal may be seen. In the weld metal welded under shielding gas, no such corrosion attack was found in any of the specimens, and the copper surface under the Cu_2S film was only roughened (with matching morphology to the Cu_2S crystals of the inner film), as shown in Figure 30 d). Thus, it can be concluded that also the Cu_2O particles in the weld metal will be destabilized in the presence of dissolved sulphide ions in the solution in addition to the pre-existing oxide film.

A common feature in both weld metal specimens, shown in Figure 31, was that the Cu_2S film was not continuous and there were openings revealing the Cu surface. In the middle of these openings, there was always a particle that had corroded. The particles were analysed by EDS and their corrosion products always contained iron (Fe) and nickel (Ni) oxides and sulphides. It can be concluded that these Fe/Ni rich particles most likely are debris of the tool wear, which were embedded in the weld metal during the welding process. Sometimes plenty of Fe rich corrosion products had formed filling the whole opening in the Cu_2S film. This is shown in Figure 31 d).

In the low sulphide solution, very similar thin Cu_2S film formed on the weld metal surfaces as on the base material. However, typical for the weld metals was that the specimens showed small surface defects, shown in Figure 32 a), both in specimens welded in air and in the shielding gas, which are clearly visible on the surface in addition to the grinding marks. In pre-oxidized condition, the surface film was uneven and contained much porosity, visible as holes in the film in Figure 32 b). In the low sulphide conditions, corrosion attack on oxide stringers in the weld metal, welded in air, and on particles left from the tool wear, was not found, as in the specimens exposed to the high sulphide containing solution.

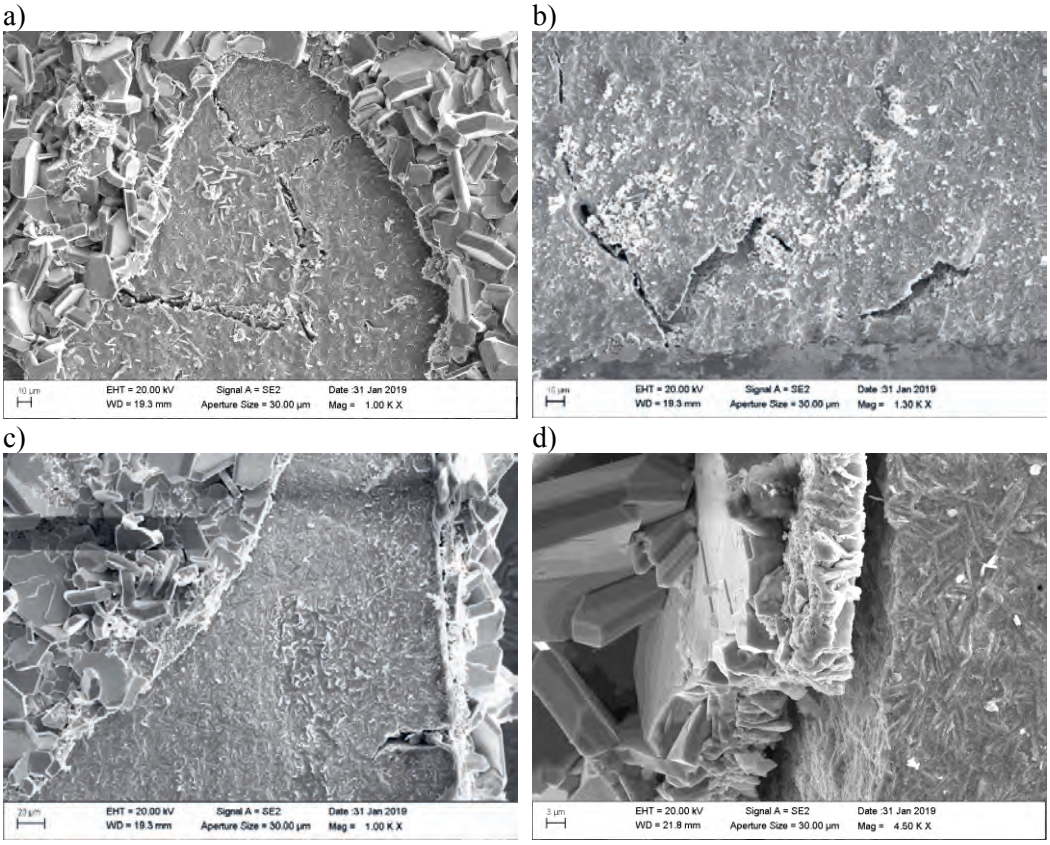

Figure 30. Surface morphology and cross-section of the Cu_2S film, as well as attacked oxide particles on the Cu surface under the film after four weeks exposure in 0.001 M Na_2S solution at 90°C. Coupon specimens a), b) and c) 1W1_ox_HS, and d) 2W1_ox_HS.

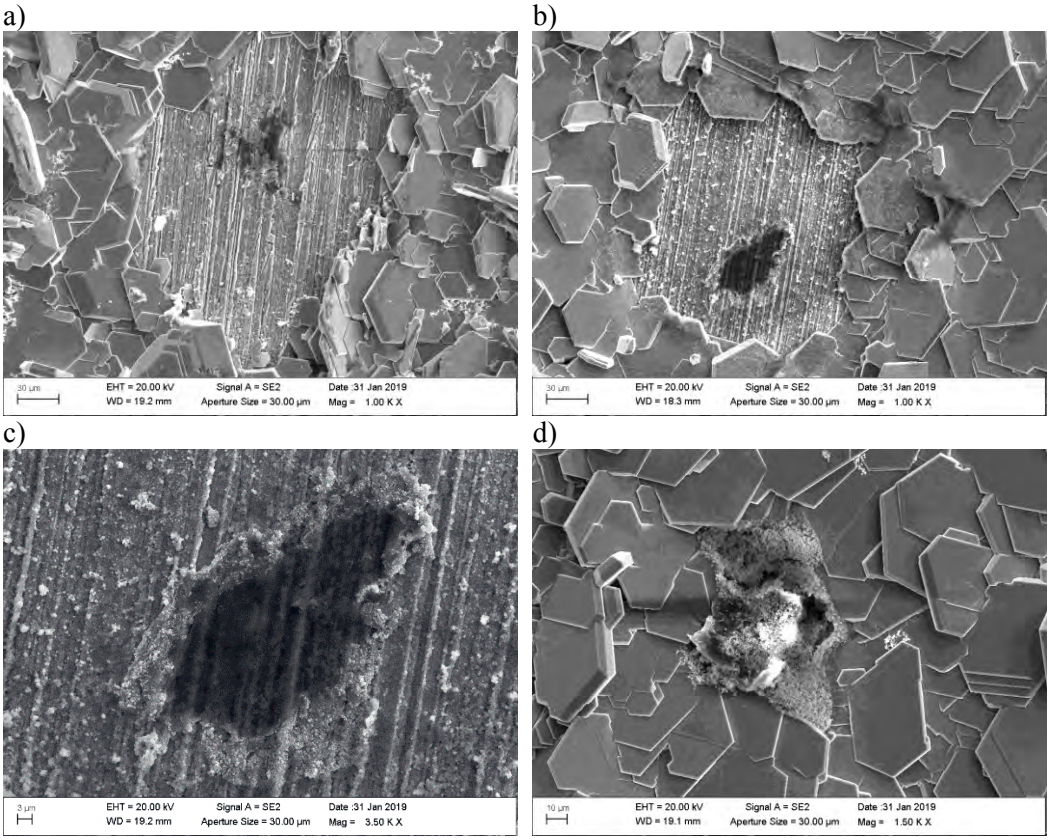

Figure 31. Openings in the Cu_2S film on the weld specimens are related to Fe/Ni rich particles embedded in the weld metal. The particles were locally attacked during the four weeks exposure in 0.001 M Na_2S solution at 90°C. Coupon specimens a) 1W1_ox_HS and b), c), d) 2W2_HS.

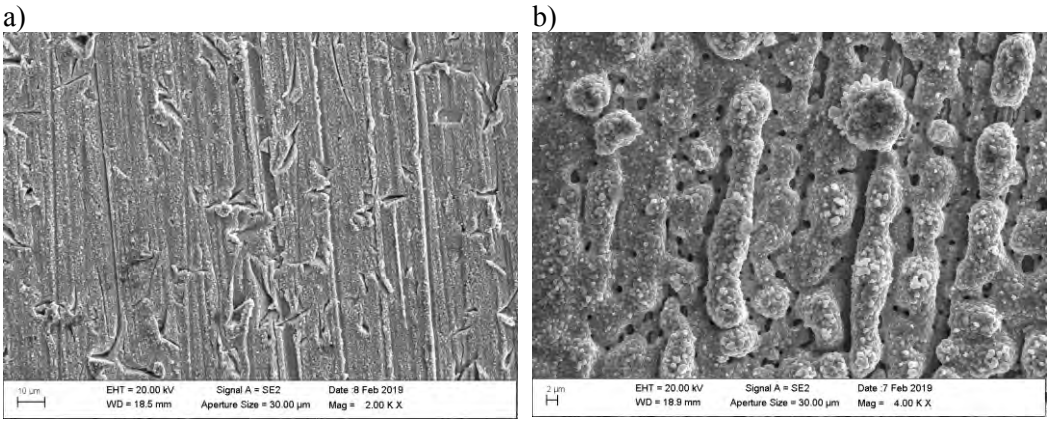

Figure 32. Surface morphology of the Cu_2S film and defects on the weld metal surface, as well as porosity of the film after four weeks exposure in 0.00001 M Na_2S solution at 90°C. Coupon specimens a) 2W3_LS, and b) 2W1_ox_LS.

3.4. Results of hydrogen thermal desorption spectroscopy (TDS)

Temperature dependencies of hydrogen desorption rates measured after SSRT in the high sulphide environment, and for the unloaded coupons exposed in the high sulphide environment, are shown in Figures 33 and 34, respectively. The desorption curve for the as-supplied state is shown for comparison purposes. The graphs manifest a distinctive desorption peak of hydrogen in the temperature range of 550 to 850 K. The peaks consist of, at least, two overlapping components, which are more visible in the as-supplied state.

There are two significant findings of the TDS measurements. First, an increase of hydrogen content in all TDS samples cut from SSRT specimen #8, tested in 0.001 M sulphide environment, has occurred when compared to hydrogen content in the as-supplied state. Specimens S1_G1_HS and S1_G2_HS were cut from the gauge section, and specimens S1_S_HS and S1_L_HS were cut from the threaded ends of the tensile specimen (Figure 33). S1_G1_HS, which was cut from the narrow gauge-section, contains the most hydrogen, possibly because it experienced the most deformation. The second finding concerns the hydrogen uptake in the unloaded FSW weld metal measured after exposure in the 0.001 M sulphide environment. As seen in Figure 34 a), the copper specimen welded in air (1W3_HS, green curve) manifests almost three times higher hydrogen content than the material welded in the protective atmosphere (2W3_HS, blue curve). This indicates that the copper oxide (Cu_2O) particles, which form in the FSW process in the presence of oxygen and are mixed in the bulk of copper, act as strong trapping sites for hydrogen. Moreover, a great number of hydrogen partial pressure spikes is observed on the low-temperature side of the TDS peak, evidencing that hydrogen forms gas-filled voids at the Cu_2O particles, some of which are located close to the specimen surface and open suddenly due to increasing gas pressure with increasing temperature. Magnification of some of the spikes is shown Figure 34 b).

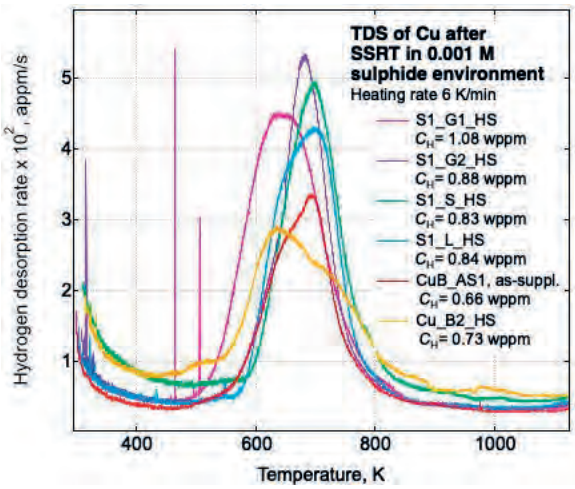

Figure 33. Temperature dependencies of hydrogen desorption rate for samples cut from tensile specimen #8 after SSRT in 0.001 M sulphide environment. Samples cut from the gauge section are named S1_G1_HS and S1_G2_HS. Samples cut from the threaded ends are named S1_S_HS and S1_L_HS. Unloaded copper coupon subjected to the same environment is named B2_ox_HS, and unexposed reference sample in as-supplied state is named B_AS1.

a) b)

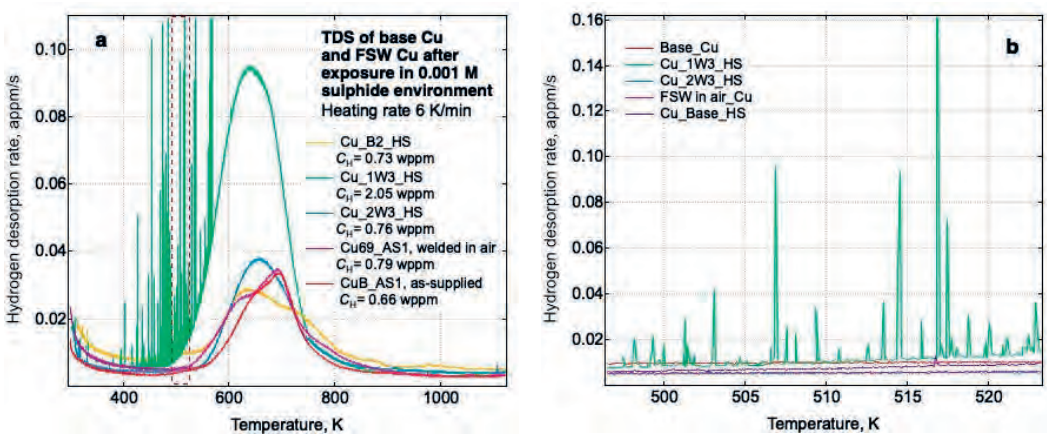

Figure 34. a) Temperature dependencies of hydrogen desorption rate for samples cut from the unloaded coupons of FSW copper welded in air (1W3_HS) and in protective atmosphere (2W3_HS), as well as for the base copper (B2_ox_HS) after exposure in 0.001 M sulphide environment. The reference samples in as-supplied state are named B_AS1 for the base material and 69_AS1 for the weld metal welded in air. b) Magnification of desorption spikes marked in a) with the red dashed box.

Figure 35 a) shows the hydrogen desorption curves of TDS samples cut from the SSRT specimen #9, and b) cut from the unloaded coupons of Cu-OFP tested in the same low sulphide environment. They manifest a rather different behaviour when compared to copper tested in the high sulphide environment. As expected, the exposure of copper in the low sulphide environment results in reduced hydrogen uptake, which was not clear in the previous short time testing of two weeks [3], but still hydrogen concentration in the samples cut from the SSRT specimen #9 after plastic deformation is higher than that of the unloaded coupons of the base material or argon shielded weld after exposure in the same environment.

Comparison of Figure 35 b) and Figure 34 a) shows that hydrogen uptake in the unloaded copper coupons in 0.00001 M sulphide environment is markedly reduced when compared to exposure in the high sulphide environment. Note that the scale of hydrogen desorption rate is different in the two graphs. In the samples exposed to the low sulphide environment, no spikes were observed on the low temperature side of the TDS curves of FSW copper welded in air. However, hydrogen concentration in this sample (1W4_LS2) was still somewhat higher than that in the coupon of the FSW copper welded with protective atmosphere (2W4_LS2).

a) b)

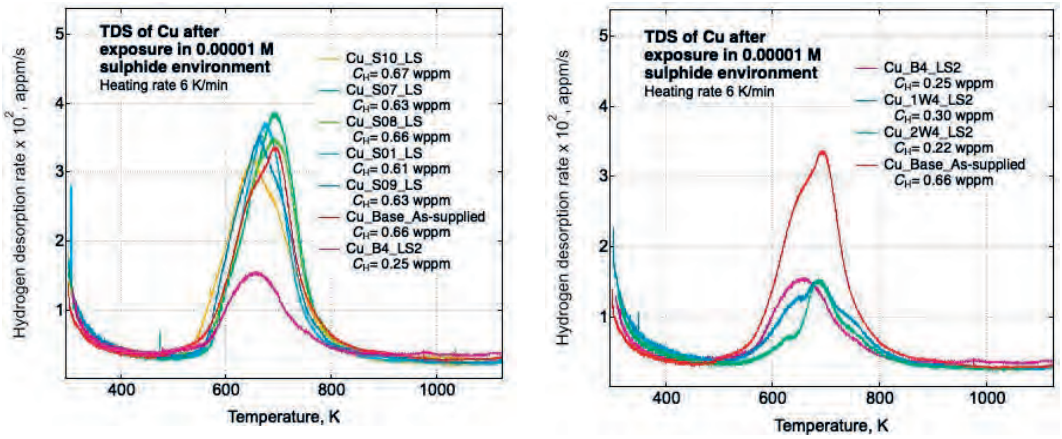

Figure 35. a) Temperature dependency of hydrogen desorption rate for samples cut from tensile specimen #9 after SSRT in 0.00001 M sulphide environment. Samples S07_LS, S08_LS and S10_LS were cut from the gauge section and samples S01_LS and S09_LS from the threaded ends. Unloaded base copper exposed in the same environment is marked with B4_LS2, and the reference sample in as-supplied state with Cu_Base (=B_AS1). b) Hydrogen desorption rate for samples cut from the unloaded coupons of base copper (B4_LS2) and FSW copper welded in air (1W4_LS2) and under shielding gas (2W4_LS2), measured after exposure in 0.00001 M sulphide environment, as well as for the reference sample in the as-supplied state.

It is important to notice that the hydrogen content in the unloaded copper coupons after exposure in the low sulphide environment is markedly reduced when compared to the as-supplied base material (see Figure 35 b). Such behaviour originates possibly from the fact that the autoclave tests were performed at an elevated temperature of 90°C. So-called metallurgical hydrogen is always present in copper and it can diffuse out of the sample, if the low sulphide environment does not provide hydrogen with high enough fugacity. The low fugacity of hydrogen is evidenced by the absence of spikes in the TDS curve of the FWS sample welded in air and exposed in the low sulphide environment; hydrogen gas (H_2) filled voids may form at the Cu_2O particles only in the presence of hydrogen of high enough fugacity. The hydrogen contents in the TDS samples cut from the SSRT specimen #9 were similar to the as-supplied state, but still higher than in the unloaded coupon specimens. This further indicates that plastic deformation enhances the hydrogen uptake in the SSRT specimen.

Finally, the copper Cu_2S film was removed from the surface of one coupon specimen exposed to the high sulphide environment and measured for hydrogen content. Figure 36 shows the partial pressures of hydrogen and water vapor in the Cu_2S powder. It is seen, that the powder contains hydrogen as a consequence of corrosion reactions of copper in the sulphide containing environment, as well as a small amount of water.

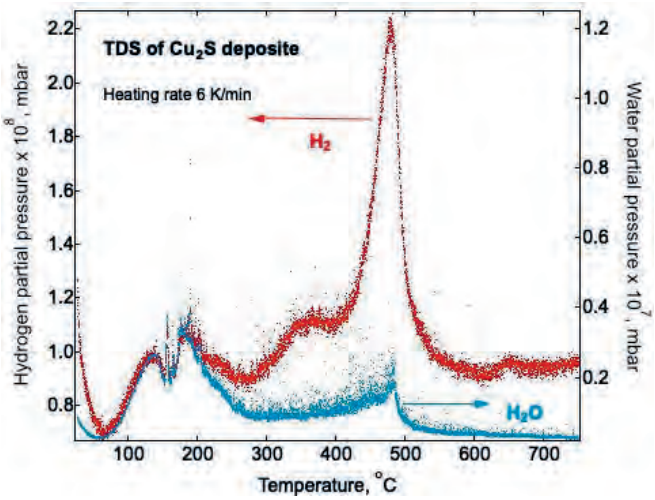

Figure 36. Temperature dependency of partial pressure of hydrogen (red curve) and water vapor (blue curve) in Cu_2S powder detached from unloaded coupon of base copper after exposure in 0.001M sulphide environment.

For further analysis, the hydrogen contents of each specimen were calculated as area under the TDS curves, some of them shown in Figures 33-35. An overview of the hydrogen contents is shown visually in Figure 37 and numerically in Table 3. Coupons of base material are marked with B(n), coupons of FSW made in air are marked with 1W(n), and coupons of FSW produced in protective atmosphere are marked with 2W(n), where (n) represents the number of the coupon specimen, as several TDS samples were cut from some of the coupons. Samples cut from the SSRT specimens are marked with S(n).

Figure 37 visualizes the above conclusion, that in general the samples exposed at the higher sulphide level have a higher hydrogen content when compared to the samples exposed at the lower sulphide level. The mechanically loaded samples in both sulphide conditions show the highest hydrogen content in the narrow gauge section (1.08 wt.ppm in high sulphide and 0.67 wt.ppm in low sulphide conditions) compared to the wide gauge section (0.88 wt.ppm and 0.65 wt.ppm, respectively, for the high and low sulphide conditions) and the threaded sections showing the lowest values (0.84 wt.ppm and 0.62 wt.ppm, respectively). Although the differences in low sulphide conditions are within the limits of the measurement technique (0.02 wt.ppm), the high sulphide specimens seem to suggest that the hydrogen uptake is dependent on the level of deformation. However, the number of samples was limited, and the results should thus be viewed in the light of this.

It should be noted, that the highest hydrogen content of 1.58-2.05 wt.ppm was measured in the FSW weld metal welded in air and tested in the high sulphide environment. The hydrogen content of the specimens welded in air is more than that in the mechanically loaded SSRT specimen tested in the same environment (0.83-1.08 wt.ppm). This may be explained by the oxide particles in the air welded copper functioning as hydrogen trapping sites and possibly reacting with the sulphide solution. Thus, the air welded copper is a special case. In general, the samples cut from the mechanically loaded specimens contained more hydrogen than the unloaded base material coupon specimens tested in the same environment. In the high sulphide environment, the average hydrogen content of the unloaded coupons (excluding the air welded specimens due to the above-mentioned reason) is 0.77±0.11 wt.ppm, whereas in the SSRT specimen it is 0.91±0.09 wt.ppm. This difference is more evident in the low sulphide conditions as the coupon specimens (again excluding the air

welded specimens) contained on average 0.29±0.06 wt.ppm hydrogen, but the plastically deformed SSRT specimen contained on average 0.64±0.02 wt.ppm hydrogen. The hydrogen content of the coupon specimens tested in the low sulphide environment was reduced from the initial base material state (which was 0.66 wt.ppm), but this may be explained by the outgassing due to the elevated temperature of 90°C and low fugacity of hydrogen in the low sulphide conditions. Still, the higher hydrogen content in the SSRT specimen, when compared to the mechanically unloaded coupons tested in the low sulphide environment, further indicates that plastic deformation of copper enhances the hydrogen uptake, resulting in these tests in similar hydrogen content in the SSRT specimen as in the as-supplied state. In the high sulphide conditions hydrogen absorption in the unloaded coupon specimens (excluding the air welded specimens) was negligible, except for specimen B3_HS, but on average plastic deformation still increased the hydrogen absorption in the high sulphide environment as well.

The exact trapping sites of hydrogen in copper are still unknown. However, the TDS peaks appear most likely due to hydrogen de-trapping from energetically deep trapping sites in the copper crystal lattice, such as vacancies and vacancy complexes. The obtained TDS results suggests that plastic deformation of Cu-OFP in the sulphide environment enhances the generation of not only the excessive hydrogen, but also the corresponding crystal lattice defects forming in plastic deformation. However, verification of the above hypothesis still needs additional studies.

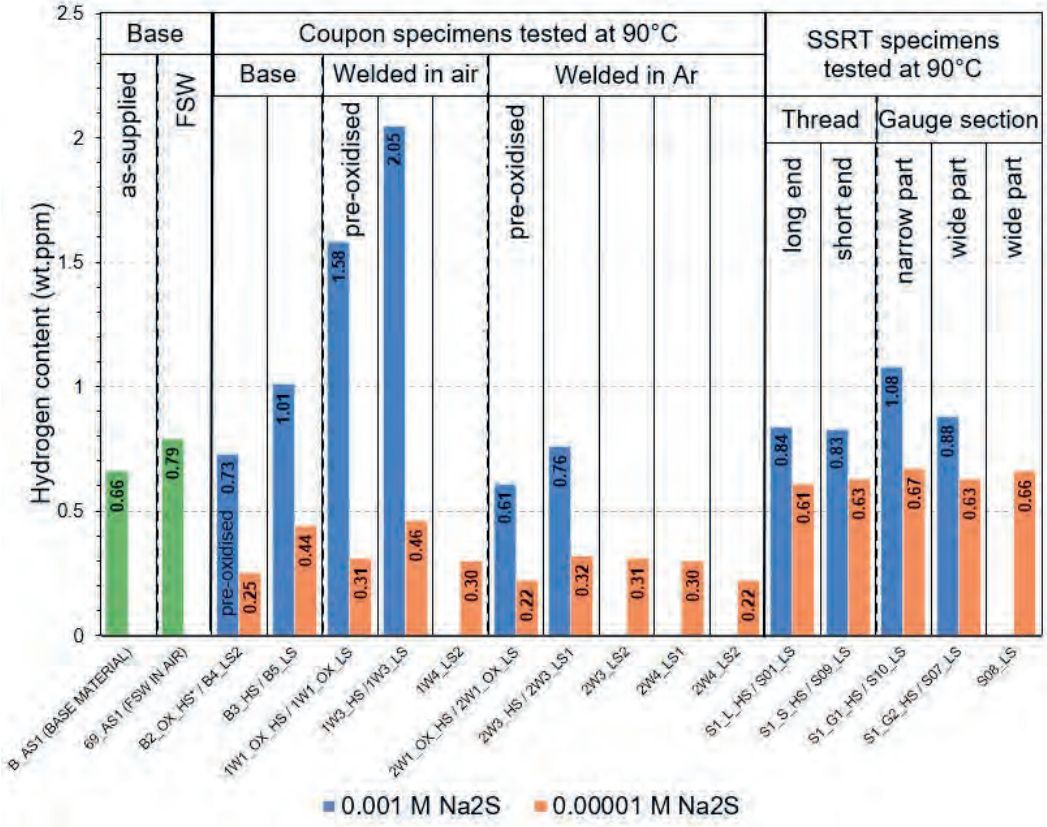

Figure 37. Hydrogen contents of base materials, coupon specimens, and SSRT specimens tested in the two different sulphide environments at 90°C.

Table 3. *Hydrogen contents measured with TDS from samples cut from the SSRT specimens and from the coupon specimens, as well as from the as-supplied Cu-OFP lid material and as-welded FSW copper welded in air.*

	Sample	*Weight (g)*	*Thickness (mm)*	*Hydrogen content (at.ppm)*	*Hydrogen content (wt.ppm)*
	B_AS1 (base material)	0.4333	0.890	41.86	0.66
	69_AS1 (FSW in air)	0.3419	0.880	50.26	0.79
10^{-3} M Na_2S	B1_ox_HS*	0.2988	0.980	48.2	0.76
Coupon specimens	B2_ox_HS*	0.3031	0.980	46.6	0.73
	B3_HS	0.2957	0.980	64.22	1.01
	1W1_ox_HS*	0.2969	0.986	100.13	1.58
	1W3_HS	0.3002	0.965	130.42	2.05
	2W1_ox_HS*	0.2625	0.978	38.55	0.61
	2W3_HS	0.3135	0.980	48.01	0.76
	Cu_2S powder**	0.0494	1.000	N/A	N/A
10^{-3} M Na_2S	S1_L_HS	0.2846	0.904	53.38	0.84
SSRT specimen	S1_S_HS	0.2767	0.870	53.10	0.83
	S1_G1_HS	0.3207	0.950	68.63	1.08
	S1_G2_HS	0.3332	0.970	55.92	0.88
10^{-5} M Na_2S	B4_LS1	0.3190	0.970	10.35	0.16
Coupon specimens	B4_LS2	0.2982	0.960	15.78	0.25
	B5_LS	0.2936	0.936	27.80	0.44
	1W1_ox_LS*	0.2790	0.970	19.74	0.31
	1W3_LS	0.2873	0.951	29.09	0.46
	1W4_LS2	0.3074	0.947	19.16	0.30
	2W1_ox_LS*	0.2933	0.960	14.20	0.22
	2W3_LS1	0.3057	0.963	20.49	0.32
	2W3_LS2	0.2919	0.955	19.74	0.31
	2W4_LS1	0.3342	0.970	18.75	0.30
	2W4_LS2	0.2942	0.990	14.00	0.22
10^{-5} M Na_2S	S01_LS	0.3797	0.928	38.69	0.61
SSRT specimen	S10_LS	0.3657	0.936	42.86	0.67
	S07_LS	0.3792	0.923	44.29	0.63
	S08_LS	0.3791	0.924	41.63	0.66
	S09_LS	0.3703	0.913	40.13	0.63

*Specimens pre-oxidized before the autoclave exposure;
**Amount of hydrogen in Cu_2S powder was not calculated because of lack of calibration procedure for TDS measurement of powders.

3.5. Sulphide and oxide film XRD characterization

The XRD diffractogram of the unexposed pre-oxidized specimen is shown in Figure 38. It confirms that the electrochemically deposited surface film on the specimen surface was a cuprite (Cu_2O) film (see also Figure 26). No tenorite (CuO) was present in the film. Mainly Cu peaks are visible because of the Cu substrate. The only oxide peak is the (111) Cu_2O peak. Note that the y-axis is in square root of the intensity. The amount of Cu_2O here is much below one atomic percent. The small peak at 39° 2θ is the K_β peak of the Cu(111) reflection.

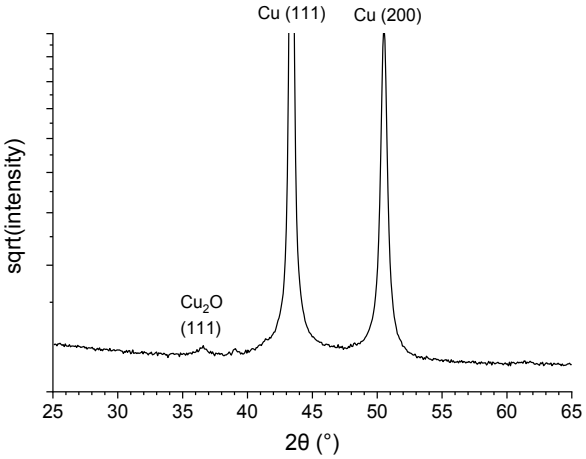

Figure 38. X-ray diffractogram of the pre-oxidized copper specimen B1_ox without exposure to the sulphide solution.

XRD measurements of three base material coupon specimens, two exposed in high sulphide environment (B3_HS and B2_ox_HS) and one exposed in low sulphide environment (B2_ox_LS) are shown in Figure 39. The peak locations coincide well for all the specimens, with the exception of copper substrate being clearly visible for the thin film formed on B2_ox_LS. There are large variations in intensities, though. This is probably due to the very large crystallites and non-random orientation of the crystallites, which leads to poor particle statistics. Major phase in all specimens appears to be monoclinic Cu_2S (ICDD PDF card 33-490). All the reflections from specimen B3_HS can be explained by that phase. CuS does not seem to be present in any of the specimens. In comparison to the other specimens, there are noticeable reflections from residual Cu_2O phase in the pre-oxidized B2_ox_HS specimen. These are marked with solid dots (ICDD PDF card 5-667). Some Cu_2O is still left on the specimen surface from pre-oxidation before conversion of the oxide film to sulphide film (see also Figure 28). CuO was not found from the pre-oxidized specimen.

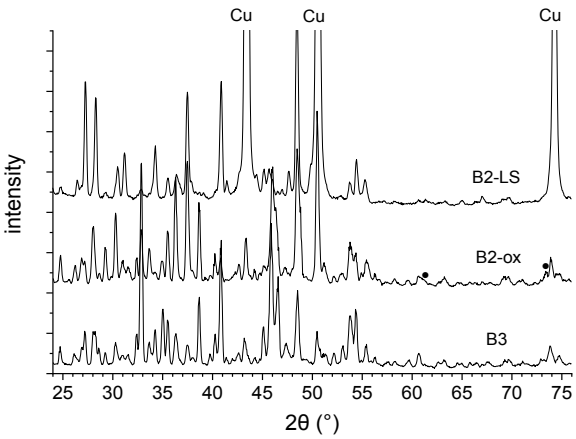

Figure 39. XRD measurement of Cu_2S film formed on two high sulphide coupon specimens (B3_HS and B2_ox_HS) and one low sulphide coupon specimen (B2_ox_LS).

The Cu_2S film was removed from the copper coupon B3_HS in order to better understand the composition. The film was ground to fine powder, and then measured in Bragg-Brentano geometry in order to improve the particle statistics and reduce texture related issues. The result of this measurement is shown in Figure 40. It matches well with monoclinic Cu_2S phase. However, there may be a few atomic percentages of hexagonal Cu_2S (ICDD PDF card 26-1116) present, as it slightly improves the fitting. However, the hexagonal phase should not be stable at room temperature. CuS is not present at all according to the Rietveld refinement of this measurement.

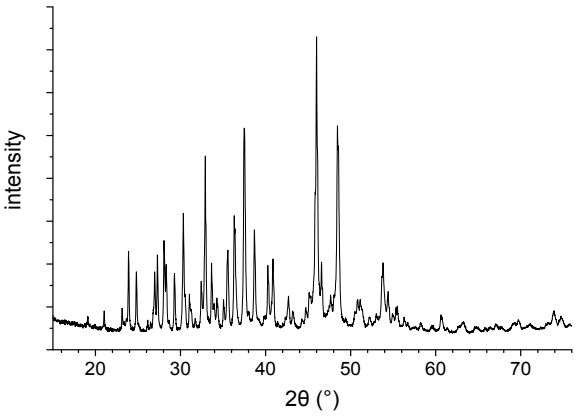

Figure 40. Powdered Cu_2S sample removed from coupon specimen B3_HS measured in Bragg-Brentano geometry.

4. Discussion

Repositories in Forsmark and Olkiluoto contain sulphide ions (SH^-) in groundwater as a product of sulphate-reducing bacteria and mineral dissolution processes (e.g., dissolution of pyrite, $4FeS_2 + 3H_2O \rightarrow 4Fe(II) + 6SH^- + S_2O_3^{2-}$) [10, 14]. Sulphide ions are the main corroding species for the copper material during expected repository conditions [15-17]. Knowledge on the characteristics of the Cu_2S film, expected to form on the spent nuclear fuel copper canisters, is essential to determine whether or not localized corrosion in the form of pitting and stress corrosion cracking (SCC) is a possible degradation mechanism. Localized corrosion requires the formation of a protective, passive film and therefore the properties of the Cu_2S film are important in a wide range of SH^- and Cl^- contents.

The copper canister will be subjected to a number of corrosion processes [14, 15]. Since the conditions will initially be oxidizing due to the presence of oxygen, trapped in before sealing of the repository, and the presence of oxidants produced by radiolysis of groundwater, there is a possibility of localized corrosion in the form of pitting and SCC. The extent of general corrosion due to this oxygen and due to radiolytic corrosion is expected to be minimal at 80-90 µm [14]. A requirement for pitting and SCC to occur is that the copper surface must be passive, and the conditions are required to support the separation of anodes and cathodes. This is a prerequisite for this form of corrosion [15-17]. Whether or not pitting or SCC occurs is a balance between factors that promote passivation and factors that lead to film breakdown and the establishment of general corrosion. Cu_2S is more stable in sulphide solutions than copper oxide, based on thermodynamic data, and therefore conversion of the pre-existing copper oxide film on the copper canister surface leads to Cu_2S formation in sulphide solutions:

$$Cu_2O\ (s) + SH^-\ (aq) \rightarrow Cu_2S\ (s) + OH^-\ (aq). \qquad (1)$$

Once anaerobic conditions are established the major corrosion mechanism is, thus, corrosion by sulphide-induced reactions. Corrosion studies in aqueous solutions containing SH^- have shown that sulphide corrosion is a two-step process where adsorption on copper occurs first to form the chemisorbed species $Cu(SH)_{ads}$ [12, 18-22]:

$$Cu + SH^- \rightarrow Cu(SH)_{ads} + e^-. \qquad (2)$$

This chemisorbed species then reacts with Cu and SH^- leading to deposition of Cu_2S on the Cu surface:

$$Cu + Cu(SH)_{ads} + SH^- \rightarrow Cu_2S + H_2S + e^-. \qquad (3)$$

Hydrogen evolution under anoxic conditions is the viable cathodic reaction:

$$2SH^- + 2e^- \rightarrow H_2 + 2S^{2-} \qquad (4)$$

This leads to H_2 formation, which occurs initially at the Cu/electrolyte interface, but shifts to Cu_2S/electrolyte interface on the conducting film once the film has grown [18-21]. Whether or not this reaction occurs partially at the copper surface at the base of the pores when porous films are present, is not known. However, the cathodic reaction provides hydrogen near or at the Cu surface, and some of the hydrogen may enter the metal as H^+.

It was observed that at low sulphide concentration, a thin porous single-layer film formed, reaching only a thickness of about 200-400 nm, whereas in the high sulphide environment,

the Cu_2S film growth occurred as two or three distinct layers. Most of the film growth occurred in this case as a much thicker, more compact, but still porous and brittle outer deposit layer. Passivation did not occur. The film consists of an inner barrier layer and an outer chalcocite (Cu_2S) deposit layer, film growth occurring at the Cu_2S/electrolyte interface [18-21]. The initial thin layer of film has grown directly from the Cu surface, which may explain the different morphology of the inner film. It was observed that deformation of the specimen due to mechanical loading leads to single-layer Cu_2S film formation and continuous detachment of the Cu_2S film from the Cu surface. A new film forms on the Cu surface under the previous one, once the previous layer has detached.

Under stagnant conditions, a parabolic growth law is observed with growth controlled mainly by Cu^+ transport in the film [19]. The high porosity facilitates the transport of Cu^+ to the film/electrolyte interface, leading to the formation of the outer Cu_2S deposit layer. This indicates, that it is the accumulation of this deposit that controls the overall film growth rate at high sulphide concentration. At lower SH^- concentrations, a linear growth law is observed leading to development of a Cu_2S film with a fine grain structure, whose growth is controlled predominantly by SH^- diffusion in the pores of the film or in the solution in transport limited conditions [19]. Thus, at low SH^- concentration, a thin, single-layer, brittle and porous, non-protective film forms. A dual-layer film develops as the SH^- concentration increases above $>5\times10^{-4}$ M and at high SH^- fluxes [12, 18-21]. The effects of chloride on copper corrosion in anaerobic sulphide solutions has also been previously studied and chloride was found to (i) inhibit Cu_2S film growth by displacing adsorbed sulphide from the copper surface; (ii) induce film porosity; and (iii) facilitate transport of Cu^+ to the solution at very high chloride concentrations [12].

Similar to [21], it was observed that the unlimited supply of SH^- leads to enhanced film growth in the form of a thick outer deposited layer, not the re-enforcement of the thin base layer. However, the interfacial reaction between Cu and SH^- is very fast [21], and therefore film thickening may lead to SH^- depletion at the copper canister surface in repository conditions. A number of electrochemical measurements indicate that formation of a passive barrier layer does not occur even at very high SH^- concentrations and high SH^- fluxes, when the overall film growth rate is controlled by the properties of the outer deposit layer [12, 18-21]. Thus, when a compacted bentonite buffer is present on the surface of the copper canister and the SH^- flux is limited, passivation of the copper canister surface probably does not occur. Pitting and SCC are therefore not expected. The separation of the Cu_2S film from the SSRT specimens tested in the low sulphide environment showed that intergranular corrosion and corrosion attack on slip lines occurred, but in general, the corroded copper surface was only roughened due to the growth of the Cu_2S crystals, not pitted.

In contrast, potentiodynamic polarization measurements of copper in deaerated sulphide and chloride containing solutions indicate that copper is passive in a wide potential range and shows passivity breakdown and hysteresis upon reversing the potential scan after breakdown has occurred, as well as shallow pitting attack [16, 17]. The high electrode potentials are not typical for the anaerobic repository conditions after the first oxic phase, but the reason for different results on copper passivity in deaerated sulphide and chloride containing solutions obtained with the different types of experiments has to be resolved to make a final judgement on this issue.

Several slow strain rate tests (SSRT) of Cu-OFP in 0.1 M NaCl containing solution with varying content of S^{2-} from 0.001 M to 0.00001 M were previously conducted in [3, 4]. The previous study showed that SCC cracking can occur at sulphide concentration of 0.001 M,

which is an order of magnitude lower than reported in [2], but still higher than the highest measured sulphide concentration in Forsmark (0.00012 M) [5]. In all studied conditions, surface defects, not positively attributed to SCC, were also present [3, 4]. The previous specimens were studied for hydrogen uptake, and the hydrogen content of copper increased from 0.5 wt.ppm to 1.2 wt.ppm during the short time SSRT testing of two weeks. This can be compared to the maximum allowed hydrogen content of copper, in the KBS-3 concept of 0.6 wt.ppm [6]. The study suggested that the SCC cracking mechanism of copper in reducing anoxic sulphide environment may be related to the hydrogen uptake, as opening of grain boundaries of copper has previously been observed in hydrogen-enhanced creep of Cu-OFP [7]. Micro-voids formed on grain boundaries positioned along maximum shear, indicating a process of accommodating the shear stress component, e.g. by grain boundary sliding [7]. On the other hand, a simulation study on hydrogen effects on void nucleation in copper showed that hydrogen stabilizes divacancies and promotes vacancy cluster formation [8]. Hydrogen prevents the collapse of large vacancy clusters. Impurities and alloying elements such as O, P, S, and Ag contribute to void formation by capturing vacancies [8].

The implications of SCC occurring at values close to the expected Forsmark sulphide levels could be severe and the SCC mechanism is still unknown. Thus, studying sulphide-induced SCC of copper in reducing, anoxic repository conditions is of great importance. The additional two exposures in this study extended the SSRT testing time up to four weeks by using lower strain rate. Intergranular defects were found at the high sulphide concentration similarly to [3, 4], but this time the defects were smaller (10-15 µm vs 70 µm), and only minor intergranular corrosion and corrosion of slip lines was found in the low sulphide conditions. Similar hydrogen uptake as in [3, 4] was confirmed to occur in the SSRT specimens. Furthermore, the amount of hydrogen uptake seems to depend on the sulphide concentration, as well as on the plastic deformation of the copper specimens. The sulphide concentration affects the fugacity of hydrogen on the copper surface, providing more atomic hydrogen near the surface as the sulphide concentration is increased. This hydrogen may be absorbed in the copper lattice as H^+ and the experimental testing suggests that plastic deformation increases this effect. Since hydrogen affinity to vacancies [8] is higher than affinity to grain boundaries or other lattice sites, a possible explanation to the enhanced hydrogen uptake due to plastic deformation may be the formation of vacancies in plastic deformation and simultaneous absorption of hydrogen in these lattice defects. This does not rule out the possible role of hydrogen in the SCC mechanism, but it seems that the main reason for hydrogen uptake in copper is the interaction of hydrogen with the lattice defects. However, the verification of this hypothesis still needs additional studies.

A number of mechanically unloaded corrosion coupon specimens were exposed simultaneously to the same environments as the SSRT specimens to study Cu_2S film formation and hydrogen uptake in the unloaded condition. In low sulphide conditions the hydrogen content of the coupon specimens was decreased from the initial state, indicating outgassing of hydrogen in the elevated temperature of 90°C. However, plastic deformation of the SSRT specimen still resulted in increased hydrogen content when compared to the unloaded condition. Several FSW weld metal specimens were exposed simultaneously, showing that if FSW is performed in air, the oxide stringers in the weld metal become destabilized and react selectively with the sulphide environment. The air-welded coupon specimens showed the highest hydrogen content of 1.58-2.05 wt.ppm (compared to 0.83-1.08 wt.ppm in the SSRT specimen), indicating an enhanced affinity of hydrogen in air welded FSW copper to the Cu_2O particles in the weld metal. It should be noted, that similar hydrogen absorption in the oxide zone of air welded FSW copper in thermal hydrogen charging

was observed in [23]. The effect should be further studied to investigate, for example, how deep in the weld metal the oxide particles are sulphidised.

Some of the coupon specimens were also pre-oxidized to reveal the conversion of the oxide film to a sulphide film. After testing, the Cu_2S films of the pre-oxidized specimens were very similar to the Cu_2S films formed on the non-pre-oxidized specimens, indicating that the transformation from Cu_2O to Cu_2S occurs quickly and almost 100% completely. Beneath the Cu_2S film, the copper surface was roughened due to the growth of the Cu_2S crystals from the copper surface, but not pitted. No intergranular corrosion was visible in any of the unloaded coupon specimens.

5. Conclusions

The testing was performed at sulphide concentrations of 0.001 M and 0.00001 M using lower strain rate than in [3, 4], which lead to testing time of four weeks in comparison to two weeks of the earlier studies. Intergranular SCC of copper in sulphide and chloride containing deoxygenated water at 90°C in reducing anoxic conditions was found to occur at sulphide concentration of 0.001 M, which is an order of magnitude lower than reported in [2], but similar to results reported in [3, 4]. The EBSD cross-section analysis of the defects show that they grow most preferably on random high-angle grain boundaries. Thus, Cu corrosion occurs more preferably on the grain boundaries than on the rest of the Cu surface when the specimen is loaded in tension. The defects become filled by the corrosion products as the adsorbed species $Cu(SH)_{ads}$ transforms into Cu_2S, making visual detection of these defects difficult without removal of the film. No similar opening of grain boundaries was found at the lower sulphide concentration, but the specimen surfaces were still slightly corroded on many grain boundaries and slip lines. The opening of the grain boundaries in the high sulphide environment may be attributed to SCC, since no similar surface defects were found in the unloaded specimens exposed to the same environment, meaning that it is not only the corrosion of Cu, but the combination of the stress state and corrosion that dictates the formation of these defects.

After the slow strain rate tensile testing (SSRT), the specimens were measured for hydrogen uptake with thermal desorption spectroscopy (TDS). The SSRT specimen tested at the high sulphide concentration of 0.001 M contained an elevated hydrogen content of up to 1.1 wt.ppm, which is almost twice the allowed hydrogen content of 0.6 wt.ppm [6]. The as-supplied base material was measured to contain 0.66 wt.ppm hydrogen, which increased to 0.73-1.01 wt.ppm after exposure in the high sulphide environment. Similarly, at the low sulphide concentration of 0.00001 M the hydrogen content of the SSRT specimen was higher than that of the unloaded coupon specimens tested in the same environment (0.61-0.67 wt.ppm compared to 0.25-0.44 wt.ppm). In this instance, the hydrogen content of the unloaded specimens was reduced from the as-supplied state, indicating that outgassing of hydrogen occurred in the low sulphide solution at 90°C, but the increased hydrogen content of the SSRT specimen tested in the same environment is a clear indication that the hydrogen uptake is related to the plastic deformation of copper. In addition to the above conclusion, it was found that the air-welded FSW weld metal shows an increased hydrogen absorption. The highest hydrogen content of up to 2.05 wt.ppm was measured in the air-welded specimen exposed to the high sulphide environment, due to hydrogen trapping and sulphidation of the oxide particles in the weld metal.

The hydrogen uptake in tensile loading is most likely related to the deformation mechanisms of copper. The uptake may be related to hydrogen dislocation interactions, as hydrogen is known to affect the dislocation dynamics of copper [7], or hydrogen vacancy interactions, as hydrogen is known to stabilize vacancies in copper [8]. Further studies, such as activation energy analysis of the trapping sites is needed to confirm this hypothesis, but the performed TDS measurements clearly evidence that plastic deformation results in increased hydrogen uptake. If the cathodic reaction provides hydrogen on the copper surface and plastic deformation, in turn, results in generation of vacancies, the formation of vacancy complexes may be further enhanced by the presence of hydrogen [8]. Since the vacancies and vacancy complexes are effective trapping sites for hydrogen, as measured by positron annihilation spectroscopy (PAS) in [24], it seems that their excessive generation in deformation and stabilization by hydrogen leads to enhanced hydrogen uptake in copper in plastic deformation in sulphide containing solutions. In addition, the hydrogen-induced vacancies and their complexes may form voids, presumably at the grain boundaries (similar to [4]), and possibly later lead to opening of the grain boundaries. Hydrogen of high fugacity is known to result in cracking of grain boundaries of Cu-OFP in tensile loading [7], but the fugacity of hydrogen in the current tests was much lower and the environment was also markedly different. Thus, the surface defect formation on the grain boundaries is most likely related to corrosion of Cu, rather than hydrogen embrittlement of the grain boundaries.

It was observed that sulphide ion concentration has a significant influence on the morphology and properties of the Cu_2S film formed on the copper surface. When the concentration is low, a fine cellular film forms. Its growth kinetics is likely linear and primarily controlled by SH^- diffusion in the aqueous solution [19]. When the SH^- concentration is high, the film appears to be more compact and likely follows a parabolic growth law [19]. In this case, the film growth is controlled mainly by diffusion of Cu^+ through the Cu_2S film, and partly by SH^- diffusion in the solution [19]. The corrosion film on the unloaded copper specimens was quite uniform and only small local holes were observed. No signs of pitting, microgalvanic corrosion [12], or intergranular corrosion were observed in the unloaded coupon specimens, but the corroded copper surface under the film was roughened. No signs of chloride were detected by EDS in the cross-sections of the studied films.

Cu_2S film growth process on the copper surface, passivation, and whether or not this can lead to film breakdown and the initiation of pitting corrosion and intergranular SCC is an important issue to be solved for copper in anaerobic sulphide solutions. The Cu_2S film, which forms at the low corrosion potentials, may convert to a more passive CuS film if the corrosion potential becomes more positive. This did not occur in these experiments because of stable and low corrosion potential of the specimens. XRD measurements also confirmed the absence of CuS.

The results of this study deepen the understanding of sulphide-induced SCC, intergranular defect formation, hydrogen uptake, and sulphide film formation on the copper surface in reducing sulphide containing anoxic conditions, which prevail in the repository for centuries after the short aerobic phase in the beginning of the disposal of the spent nuclear fuel. However, some aspects of these phenomena are still unknown and thus further studies should be conducted to understand the significance of these phenomena to the spent nuclear fuel disposal concept. Especially for the FSW weld metal, the hydrogen absorption mechanism, SCC mechanism, and sulphidation of the oxide particles should be investigated to assess their significance from the view point of spent nuclear fuel disposal.

References

1. F. King, R. Newman, Stress Corrosion Cracking of Copper Canisters. SKB Report TR-10-04, December 2010.
2. N. Taniguchi, M. Kawasaki, Influence of Sulfide Concentration on the Corrosion Behavior of Pure Copper in Synthetic Seawater. Journal of Nuclear Materials, 379(2008), 154-161.
3. R. Becker, J. Öijerholm, Slow Strain Rate Testing of Copper in Sulfide Rich Chloride Containing Deoxygenated Water at 90°C. SSM Report 2017:02, January 2017.
4. A. Forsström, R. Becker, J. Öijerholm, Y. Yagodzinskyy, H. Hänninen, J. Linder, Hydrogen Absorption in Copper as a Result of Corrosion Reactions in Sulphide and Chloride Containing Deoxygenated Water at 90°C in Simulated Spent Nuclear Fuel Repository Conditions. EUROCORR 2017, 20th International Corrosion Congress & Process Safety Congress 2017, September 3-7, 2017, Prague, Czech Republic.
5. Svensk Kärnbränslehantering (SKB), RD&D Programme 2016. Programme for Research, Development and Demonstration of Methods for the Management and Disposal of Nuclear Waste. Stockholm: The Swedish Nuclear Fuel and Waste Management Company. FUD-program 2016, September 2016.
6. Svensk Kärnbränslehantering (SKB), Programme for Research, Development and Demonstration of Methods for the Management and Disposal of Nuclear Waste. Stockholm: The Swedish Nuclear Fuel and Waste Management Company. FUD-program 2013, September 2013.
7. Y. Yagodzinskyy, E. Malitckii, T. Saukkonen, H. Hänninen, Hydrogen-Enhanced Creep and Cracking of Oxygen-Free Phosphorus-Doped Copper. Scripta Materialia, 67(2012), 931-934.
8. M. Ganchenkova, Y. Jagodzinskyy, V. Borodin, H. Hänninen, Effects of Hydrogen and Impurities on Void Nucleation in Copper: Simulation Point of View. Philosophical Magazine. 94(2014), 3522-3548.
9. P. Aaltonen, Y. Yagodzinskyy, T. Saukkonen, S. Kilpeläinen, F. Tuomisto, H. Hänninen, Role of Excessive Vacancies in TGSCC of Pure Copper. Corrosion Reviews, 33(2015), 487-500.
10. T. Martino, J. Chen, Z. Qin, D. Shoesmith, The Kinetics of Film Growth and Their Influence on the Susceptibility to Pitting of Copper in Aqueous Sulphide Solutions. Corrosion Engineering, Science and Technology, 52(2017), 61-64.
11. W. Callister, D. Rethwisch, Materials Science and Engineering, 9th Ed., John Wiley & Sons, 2015.
12. J. Chen, Z. Qin, T. Martino, D. Shoesmith, Non-uniform Film Growth and Micro/Macro-galvanic Corrosion of Copper in Aqueous Sulphide Solutions Containing Chloride, Corrosion Science, 114(2017), 72-78.
13. K. Savolainen, Friction Stir Welding of Copper and Microstructure and Properties of the Welds, PhD. Thesis, Aalto University, 2012.
14. F. King, C. Lilja, K. Pedersen, P. Pitkänen, M. Vähänen, An Update of the State-of-the-art Report on the Corrosion of Copper under Expected Conditions in a Deep Geologic Repository. Posiva report 2011-01, July 2012.
15. Hänninen, H., Forsström, A., Yagodzinskyy, Y., Copper Behavior in Geological Nuclear Waste Disposal. in *EFC "Green Book" 50 Years of Nuclear Corrosion – a Review*, 2019.
16. C. Dong, F. Mao, S. Gao, S. Sharafi-Asl, P. Lu, D. Macdonald, Passivity Breakdown on Copper: Influence of Temperature. Journal of Electrochemical Society, 163(2016), C707-C717.

17. D. Kong, A. Xu, C. Dong, F. Mao, K. Xiao, X. Li, D. Macdonald, Electrochemical Investigation and *ab initio* Computation of Passive Film Properties on Copper in Anaerobic Sulphide Solutions. Corrosion Science, 116(2017), 34-43.
18. J. Chen, Z. Qin, D.W. Shoesmith, Long-term Corrosion of Copper in a Dilute Anaerobic Sulfide Solution. Electrochemica Acta, 56(2011), 7854-7861.
19. J. Chen, Z. Qin, D.W. Shoesmith, Rate Controlling Reactions for Copper Corrosion in Anaerobic Aqueous Sulphide Solutions. Corrosion Engineering, Science and Technology, 46(2011), 138-141.
20. J. Chen, Z. Qin, L. Wu, J. Noel, D.W. Shoesmith, The Influence of Sulphide Transport on the Growth and Properties of Copper Sulfide Films on Copper. Corrosion Science, 87(2014), 233-238.
21. T. Martino, J. Smith, J. Chen, Z. Qin, J. Noel, D. Shoesmith, The Properties of Electrochemically-Grown Copper Sulfide Films. Journal of Electrochemical Society, 166(2019), C9-C18.
22. F. King, J. Chen, Z. Qin, D. Shoesmith, C. Lilja, Sulphide-transport Control of the Corrosion of Copper Canisters. Corrosion Engineering, Science and Technology, 52(2017), 210-216.
23. A. Forsström, S. Bossuyt, Y. Yagodsinskyy, K. Tsuzaki, H. Hänninen, Strain Localization in Copper Canister FSW Welds for Spent Nuclear Fuel Disposal. Journal of Nuclear Materials, 523(2019), 347-359.
24. Y. Yagodzinskyy, E. Malitckii, F. Tuomisto, H. Hänninen, Hydrogen-induced Strain Localization in Oxygen-free Copper in the Initial Stage of Plastic Deformation. Philosophical Magazine, 98(2017), 727-740.

Acknowledgements

The authors would like to thank the following persons:

Henrik Öberg (Swedish Radiation Safety Authority, SSM), who was the project contact person.

Timo Jokinen, the lead technician at Studsvik, and Riitta Johansson and Jimmy Karlsson, Studsvik, who were involved in much of the technical work during the exposures.

Johan Öijerholm and Anna-Maria Alvarez Holstein, Studsvik, for fruitful discussions during the project execution and analysis of the results.

Peter Gillen, Studsvik, who designed the autoclave control system and assisted in the autoclave maintenance.

Laura Tiainen, the laboratory technician at Aalto University, who helped with some of the SEM imaging.

Jyrki Romu, the laboratory manager at Aalto University, who was the contact person between Helsinki University and Aalto University.

Patrik Sahiluoma, Aalto University, for taking part in the sample preparation.

Appendix I: Naming of the specimens

Specimen name	Specimen type and testing environment	Notes
B_AS1	TDS sample	Base material, as-supplied
69_AS1	TDS sample	FSW in air, as-supplied
Specimen #8	SSRT specimen tested in 10^{-3} M S^{2-}	Tested simultaneously with the coupon specimens in exposure #8.
B1_ox_HS	Unloaded coupon specimens exposed in 10^{-3} M S^{2-}	base material, pre-oxidized
B2_ox_HS		base material
B3_HS		base material
B4_HS		base material
1W1_ox_HS		FSW weld metal welded in air, pre-oxidized
1W2_HS		FSW weld metal welded in air
1W3_HS		FSW weld metal welded in air
1W4_HS		FSW weld metal welded in air
2W1_ox_HS		FSW weld metal welded in argon, pre-oxidized
2W2_HS		FSW weld metal welded in argon
2W3_HS		FSW weld metal welded in argon
2W4_HS		FSW weld metal welded in argon
Cu_2S powder		Cu_2S powder removed from a coupon specimen
S1_L_HS	TDS samples cut from SSRT specimen #8 tested in 10^{-3} M S^{2-}	thread, long end
S1_S_HS		thread, short end
S1_G1_HS		gauge section, narrow part
S1_G2_HS		gauge section, wide part
Specimen #9	SSRT specimen tested in 10^{-5} M S^{2-}	Tested simultaneously with the coupon specimens in exposure #9.
B1_ox	Coupon specimen, not exposed to the sulphide environment	base material, pre-oxidized, used for XRD measurements
B2_ox_LS	Unloaded coupon specimens exposed in 10^{-5} M S^{2-}	base material, pre-oxidized
B3_LS		base material
B4_LS		base material
B5_LS		base material
1W1_ox_LS		FSW weld metal welded in air, pre-oxidized
1W2_LS		FSW weld metal welded in air
1W3_LS		FSW weld metal welded in air
1W4_LS		FSW weld metal welded in air
2W1_ox_LS		FSW weld metal welded in argon, pre-oxidized
2W2_LS		FSW weld metal welded in argon
2W3_LS		FSW weld metal welded in argon
2W4_LS		FSW weld metal welded in argon
S01_LS	TDS samples cut from the SSRT specimen #9 tested in 10^{-5} M S^{2-}	thread, long end
S09_LS		thread, short end
S10_LS		gauge section, narrow part
S07_LS		gauge section, wide part
S08_LS		gauge section, wide part

Appendix II: Exposure data

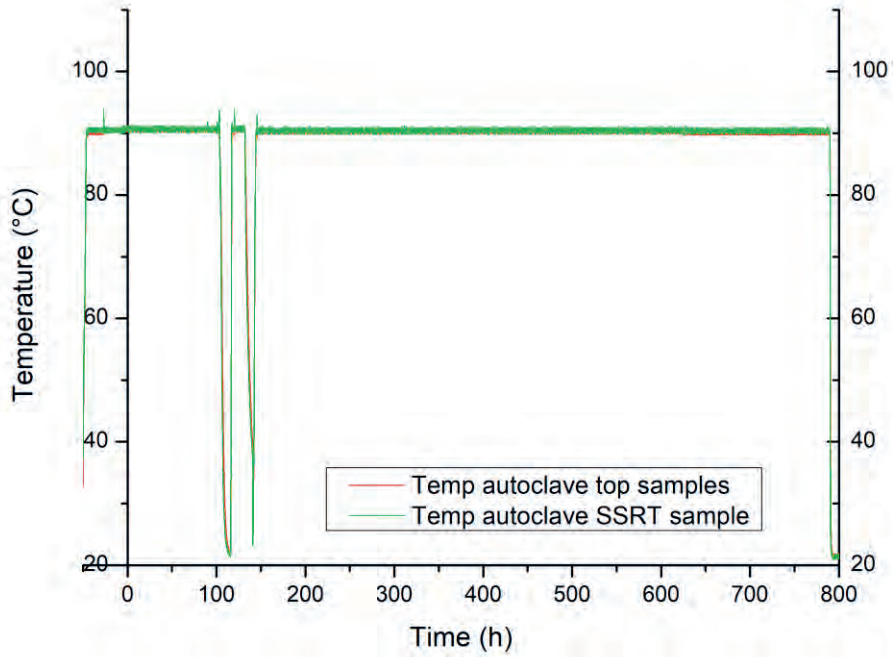

Figure B 1. *Temperature during exposure #8 (0.001 M sulphide solution).*

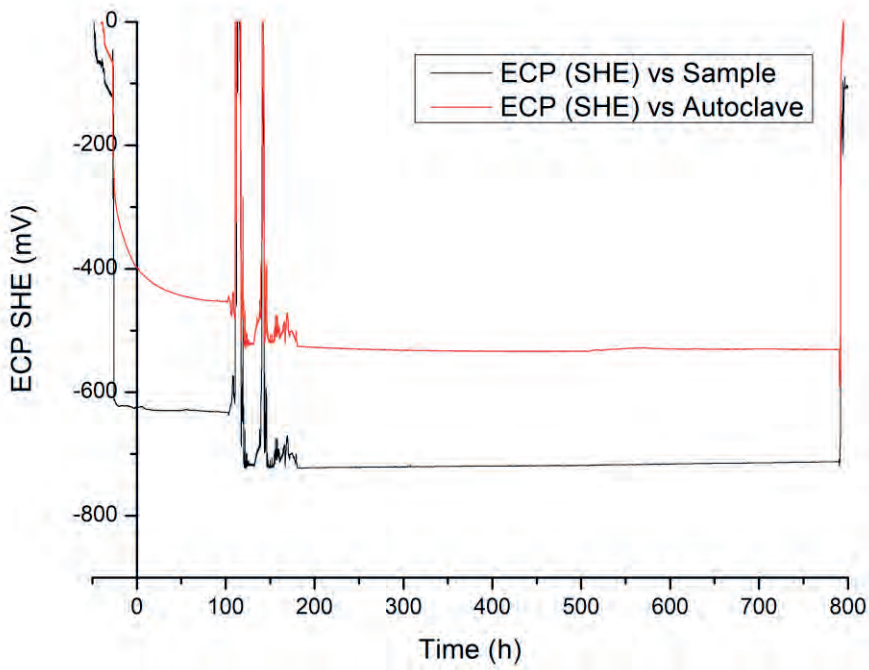

Figure B 2. *ECP during exposure #8 (0.001 M sulphide solution).*

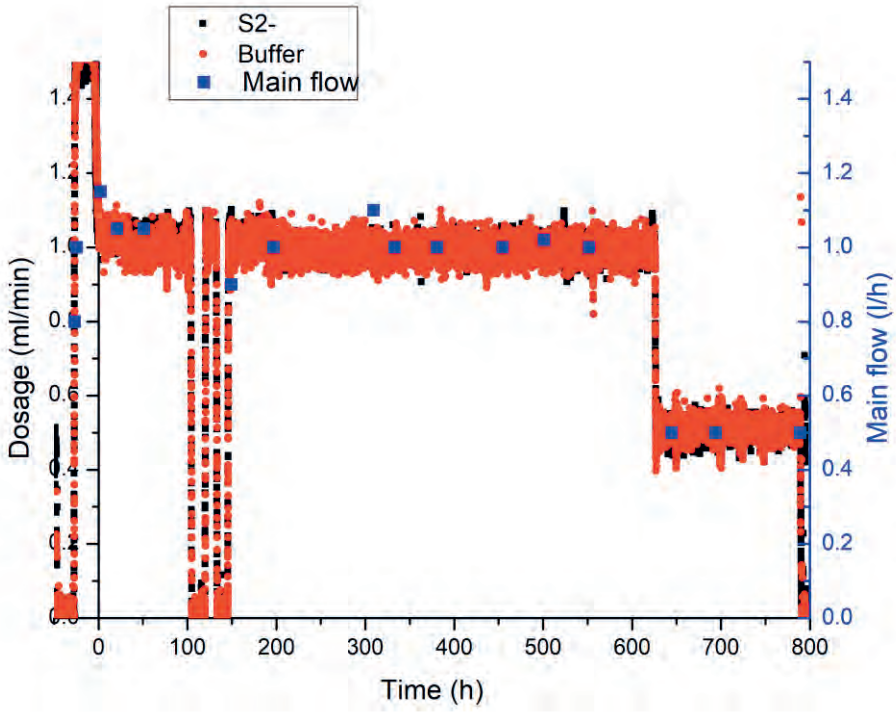

Figure B 3. *Dosage flow and main flow during exposure #8 (0.001 M sulphide solution).*

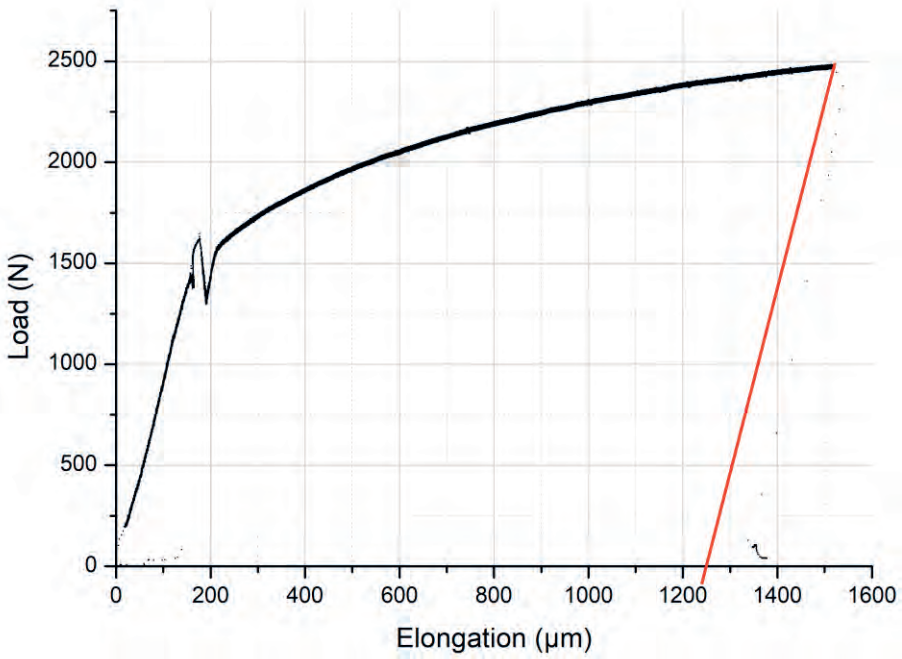

Figure B 4. *Load vs elongation during exposure #8 (0.001 M sulphide solution).*

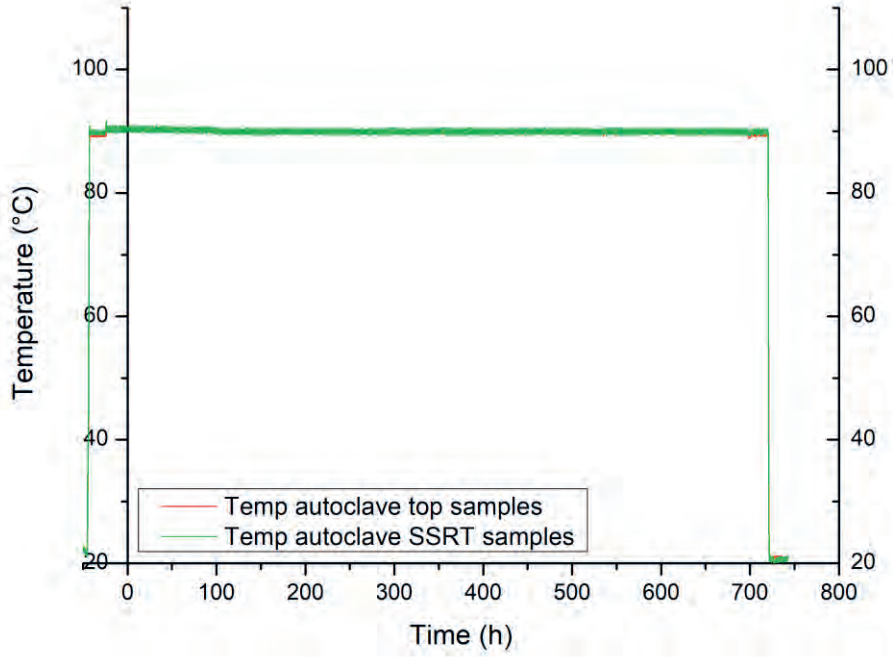

Figure B 5. *Temperature during exposure #9 (0.00001 M sulphide solution).*

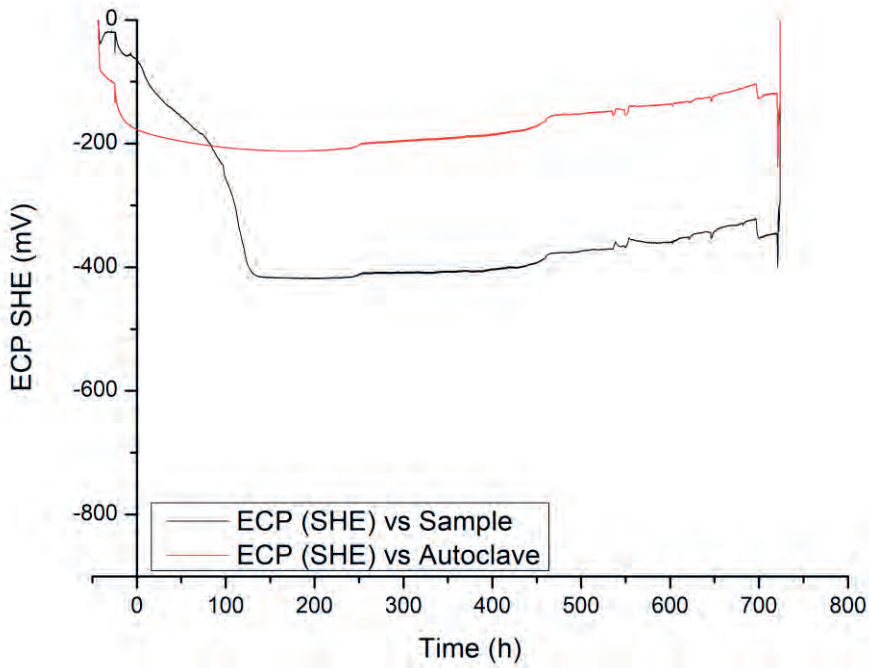

Figure B 6. *ECP during exposure #9 (0.00001 M sulphide solution).*

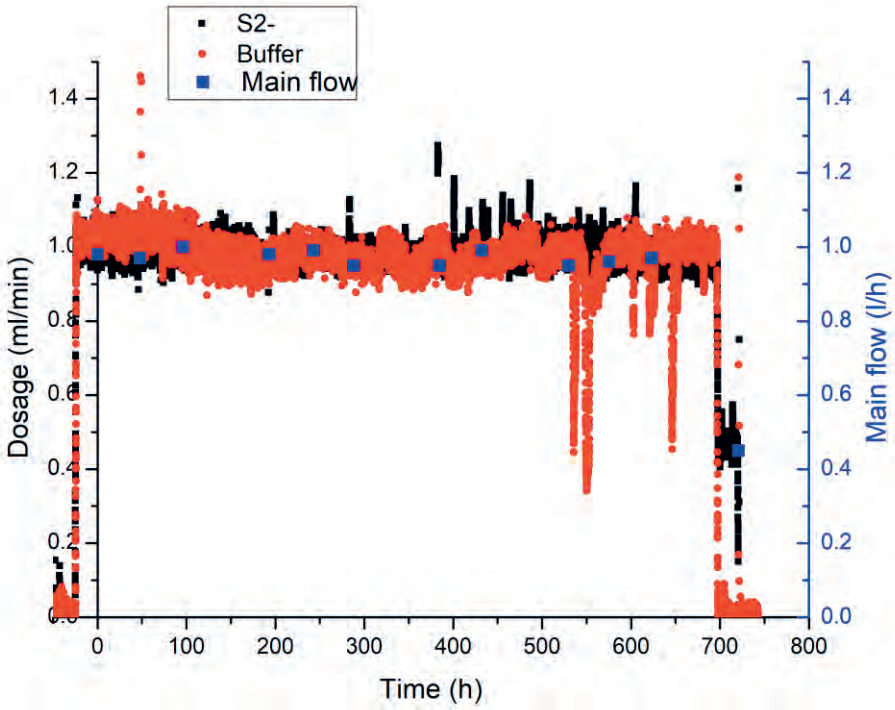

Figure B 7. *Dosage flow and main flow during exposure #9 (0.00001 M sulphide solution).*

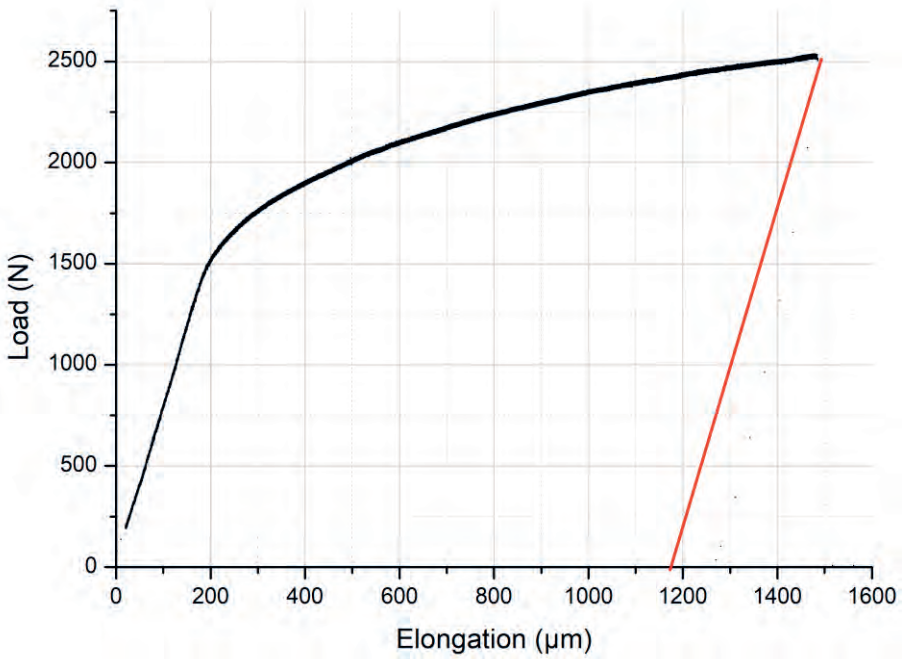

Figure B 8. *Load vs elongation during exposure #9 (0.00001 M sulphide solution).*

2020:01

The Swedish Radiation Safety Authority has a comprehensive responsibility to ensure that society is safe from the effects of radiation. The Authority works to achieve radiation safety in a number of areas: nuclear power, medical care as well as commercial products and services. The Authority also works to achieve protection from natural radiation and to increase the level of radiation safety internationally.

The Swedish Radiation Safety Authority works proactively and preventively to protect people and the environment from the harmful effects of radiation, now and in the future. The Authority issues regulations and supervises compliance, while also supporting research, providing training and information, and issuing advice. Often, activities involving radiation require licences issued by the Authority. The Swedish Radiation Safety Authority maintains emergency preparedness around the clock with the aim of limiting the aftermath of radiation accidents and the unintentional spreading of radioactive substances. The Authority participates in international co-operation in order to promote radiation safety and finances projects aiming to raise the level of radiation safety in certain Eastern European countries.

The Authority reports to the Ministry of the Environment and has around 300 employees with competencies in the fields of engineering, natural and behavioural sciences, law, economics and communications. We have received quality, environmental and working environment certification.

Strålsäkerhetsmyndigheten
Swedish Radiation Safety Authority

SE-171 16 Stockholm **Tel:** +46 8 799 40 00 **E-mail:** registrator@ssm.se
Web: stralsakerhetsmyndigheten.se

Ale Tryckteam AB, Bohus, 2020